Geodynamic Modeling of the Subduction Zone around the Japanese Islands

Satoru Honda

Earthquake Research Institute, the University of Tokyo, 1-1-1 Yayoi, Bunkyo-ku, Tokyo 113-0032, Japan
e-mail: honda@eri.u-tokyo.ac.jp

Received May 30, 2016; **Revised** October 20, 2016; **Accepted** November 16, 2016; **Online published** June 23, 2017.

Citation: Honda, S. (2017), Geodynamic modeling of the subduction zone around the Japanese Islands, *Monogr. Environ. Earth Planets*, *5*, 35–62, doi:10.5047/meep.2017.00502.0035.

Abstract In this review, which focuses on our research, we describe the development of the thermomechanical modeling of subduction zones, paying special attention to those around the Japanese Islands. Without a sufficient amount of data and observations, models tended to be conceptual and general. However, the increasing power of computational tools has resulted in simple analytical and numerical models becoming more realistic, by incorporating the mantle flow around the subducting slab. The accumulation of observations and data has made it possible to construct regional models to understand the detail of the subduction processes. Recent advancements in the study of the seismic tomography and geology around the Japanese Islands has enabled new aspects of modeling the mantle processes. A good correlation between the seismic velocity anomalies and the finger-like distribution of volcanoes in northeast Japan has been recognized and small-scale convection (SSC) in the mantle wedge has been proposed to explain such a feature. The spatial and temporal evolution of the distribution of past volcanoes may reflect the characteristics of the flow in the mantle wedge, and points to the possibility of the flip-flopping of the finger-like pattern of the volcano distribution and the migration of volcanic activity from the back-arc side to the trench side. These observations are found to be qualitatively consistent with the results of the SSC model. We have also investigated the expected seismic anisotropy in the presence of SSC. The fast direction of the P-wave anisotropy generally shows the trench-normal direction with a reduced magnitude compared to the case without SSC. An analysis of full 3D seismic anisotropy is necessary to confirm the existence and nature of SSC. The 3D mantle flow around the subduction zone of plate-size scale has been modeled. It was found that the trench-parallel flow in the sub-slab mantle around the northern edge of the Pacific plate at the junction between the Aleutian arc and the Kurile arc is generally weak and we have suggested the possible contribution of a hot anomaly in the sub-slab mantle as the origin of possible trench-parallel flow there. A 3D mantle flow model of the back-arc around the junction between the northeast Japan arc and the Kurile arc shows a trench-normal flow at a shallow depth. As a result, the expected seismic anisotropy shows the fast direction normal to the arc, even in the region of oblique subduction. This result is generally consistent with observations there. The existence of a hot anomaly in the sub-slab mantle under the Pacific plate was proposed from an analysis of the seismic tomography, and we have studied its possible origins. The origin of a hot anomaly adjacent to the cold downgoing flow, typically observed in internally heated convection, is preferable to that of a hot anomaly, such as a plume head, carried far from the subduction zone. The nature of the western edge of the stagnant slab under northeast China has been investigated with modeling studies, which take into account the subduction history and the phase changes in the mantle. It is likely to be a ridge-type plate boundary between the extinct Izanagi plate and the Pacific plate. Thus, we have concluded that the slab gap under northeast China is not a breakage of the stagnant slab. Further studies have suggested that the existence of the rheological weakening of the slab in the transition zone, and the additional effects of a hot anomaly in the sub-slab mantle under the Pacific plate, may explain the differences in slab morphology under the northern Okhotsk arc and the northeast Japan arc.

Keywords: Subduction zone, Seismic tomography, Stagnant slab, Small-scale convection, Izanagi plate.

1. Introduction: A Brief History of Subduction Zone Modelings

Plate tectonics predicts that active geologic phenomena occur along plate boundaries. Subduction zones show a variety of geologic phenomena, such as earthquakes and volcanic activities. Compared with the divergent boundary, the geologic setting in subduction zones is more complicated because of the dominance of the downward movement of a cold slab and the asymmetrical nature of the subduction processes.

Figure 1 shows examples of early models of subduction zones. McKenzie (1969) separated the subduction zone model into two regions (Figs. 1(a) and 1(b)), that is, the temperature field within the subducting slab (a modification of

doi:10.5047/meep.2017.00502.0035 ISSN: 2186-4853

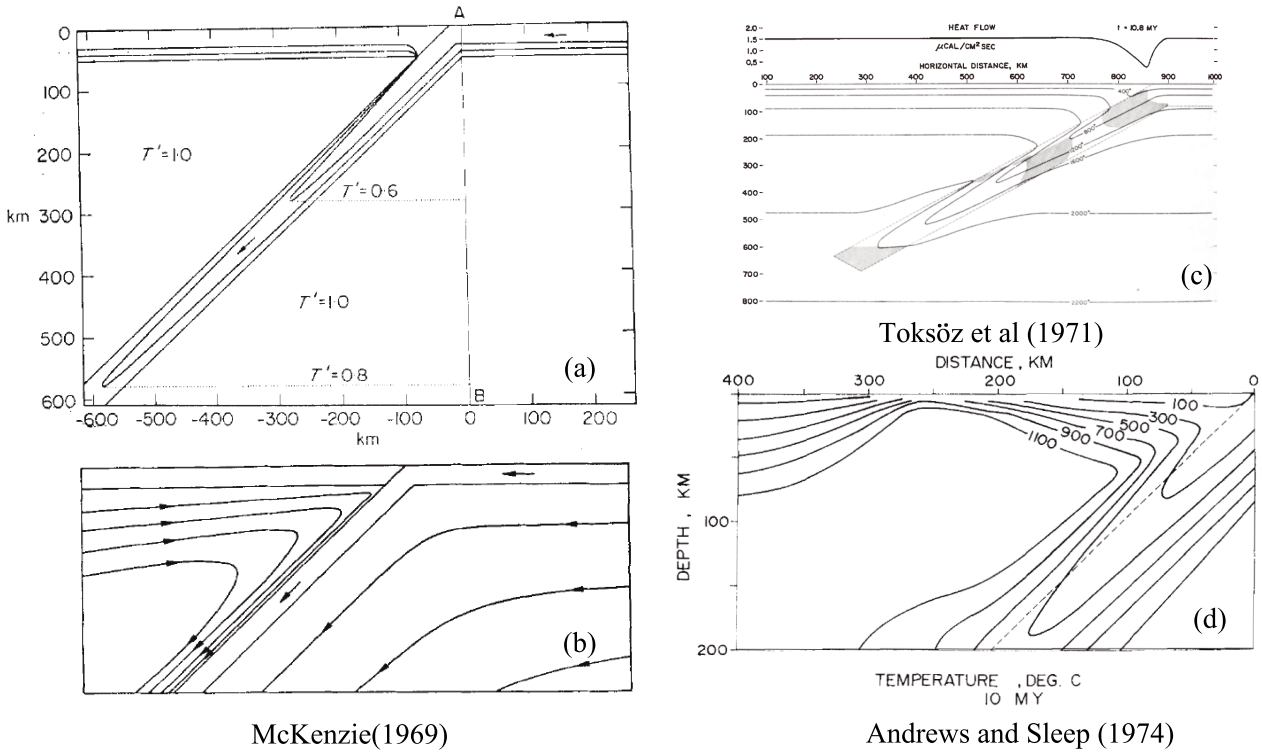

Fig. 1. Early models of subduction zones. (a) and (b) show the analytic models presented by McKenzie (1969). (c) shows the numerical model presented by Toksöz *et al*. (1971). (d) is the numerical model, which takes into account the flow in the mantle wedge, presented by Andrews and Sleep (1974).

the cooling plate model of McKenzie (1967): Fig. 1(a)) and the flow field surrounding it, (the so-called corner flow model of Batchelor (1967): Fig. 1(b)) assuming that the temperature outside the slab is well-homogenized so that the temperature and the viscosity both become constant. Based on this model, McKenzie (1969) estimated the force exerted by the negative buoyancy of the cold slab and also found the correlation between the depth of the deepest earthquakes and the (potential) temperature there. Despite the fact that his model provided a general picture of subduction zones, in order to understand the thermal processes leading to volcanic and seismic activities, it was necessary to construct more realistic models which could not be achieved by analytic methods only.

Figure 1(c) and 1(d) show examples of early numerical models of subduction zones. The model presented by Toksöz *et al*. (1971) (Fig. 1(c)) assumes the movement of the subducting slab only, and the outside of the slab the heat conduction is assumed. They estimated the importance of various possible heat sources (radioactivity, adiabatic compression, phase changes and shear heating) on the thermal structure of the subduction zones. As is evident in their results, the shallow mantle temperature, except very near the trench, is hardly affected by the slab within the time-scale of the subduction process (a few tens of a million years). This is an inevitable consequence of neglecting heat advection by flow around the subducting slab. In this type of model, the melting necessary to explain arc volcanisms is expected to occur along the upper part of the subducting slab where shear heating is assumed. The required magnitude of shear stress necessary for melting is of the order of a few hundred MPa (e.g., Minear and Toksöz (1970)).

Subsequent improvements of models were devoted to the inclusion of mantle flow around the subducting slab in numerical models. An example of such models is shown in Fig. 1(d) (Andrews and Sleep, 1974). This type of model introduces additional heat sources controlling the temperature around the subduction zone: namely, the hot mantle next to the subducting slab. This allows the melting of the mantle wedge above the subducting slab coupled with a drop in the melting temperature by fluid released from the dehydration of the subducting slab.

Usually, the last type of model consists of a given geometry and speed of the subducting slab, which are constrained by the present subduction zone, and this type of model has been commonly used for later studies of specific subduction zones (However, there is no guarantee that the geometry of the subduction in the past was the same as that in the present one.). Relaxing these constraints leads to the so-called "self-consistent model" (e.g., Tackley, 2000). Such models are certainly natural and desirable. However, it is generally difficult to compare their results with the observations of a specific region (there are, of course, exceptions in which some sort of dynamical models could explain local observations (Fukao *et al*., 2009)).

While there have been models intended to understand the generality of subduction zones, it is also useful and important to study individual subduction zones, which take into account their specific geometry, subduction history, etc. In this regard, the subduction zone around the Japanese Islands has

doi:10.5047/meep.2017.00502.0035

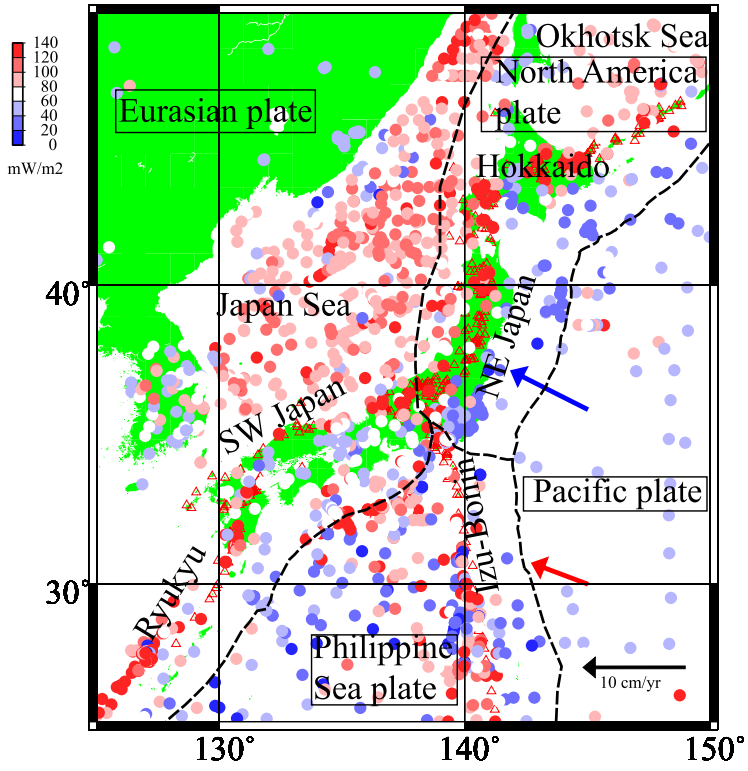

Fig. 2. Heat flow distribution around the Japanese Islands. Data from Tanaka *et al*. (2004). Dashed lines show the plate boundaries. Red triangles show the active volcanoes. Blue and red arrows show the relative motion of the Pacific plate referred to the North America plate and that referred to the Philippine Sea plate, respectively. Relative plate motions are from NUVEL1A (DeMets *et al*., 1994).

attracted the attention of many researchers, leading to many geophysical and geological studies. In the following discussions, we will consider the mechanical and thermal aspects of subduction zone modeling around the Japanese Islands.

Figure 2 shows the distribution of heat flow around the Japanese Islands, and the observation of low heat flow in the fore-arc and high heat flow in the back-arc, was considered to be a general characteristic of the subduction zone in the early days of subduction zone modeling.

Figure 3 shows examples of the chronological developments of thermal models of subduction under northeast Japan. The main purpose of the model presented by Hasebe *et al*. (1970) (left-hand column of Fig. 3) was to explain the high heat flow under the Japan Sea (i.e., the back-arc). Their model is essentially the same as that presented by Toksöz *et al*. (1971), i.e., only the slab moves. However, to account for the high heat flow under the Japan Sea by shear heating along the upper surface of the subducting slab, they assumed that, when melting occurs in the mantle wedge, the effective thermal conductivity there becomes large because of heat advection by the melt movement. In this way, they could explain the high heat flow in the back-arc within 100 Myr of subduction and with a shear stress of ∼200 MPa. They related the resultant melt production to the opening of the Japan Sea.

One interesting point is that they had to assume that the shear heating in the shallow part (shallower than D_H in Fig. 3) should be suppressed in order to account for the low heat flow in the fore-arc region. They suggested the existence of dehydration (heat sink) and/or brittleness along the slab interface (small dissipation) at depths less than D_H. Their preferred value of D_H was 60 km.

Honda (1985) modeled the flow in the mantle wedge under northeast Japan (middle column of Fig. 3). In this model, the initial and boundary temperatures under the back-arc are adjusted so that they are the consequence of back-arc spreading, which may or may not be related to the subduction of the Pacific plate. By comparing numerical results with observations, the mantle flow in the mantle wedge was constrained. A conductive upper layer (top 30 km) and a triangular region at the corner of the mantle wedge indicated by a red arrow in Fig. 3 are required, because without these settings the heat flux in the fore-arc region becomes too high, as a result of the intrusion of the hot mantle toward the surface and the corner of the mantle wedge. However, the existence of such conductive layers predicted too low a heat flow in the fore-arc region so that the landward limit of the conductive triangular region had to be adjusted and shear heating needed to be added along the interface between the conductive triangular region and the subducting plate. Honda (1985) concluded that the landward limit of the triangular region is located near the so-called "aseismic front" (Yoshii, 1975, 1979) and that a shear stress of 50 to 100 MPa was necessary. Since this model did not take into account the contribution from the radioactive heat source, the estimate of shear stress is rather high. If we assume, say ∼30 mW/m^2 of radioactive heat (e.g., Kneller *et al*., 2005), the estimate of the shear stress could be reduced to one third. It is notable that the depth of the top surface of the subducting slab beneath the aseismic

doi:10.5047/meep.2017.00502.0035

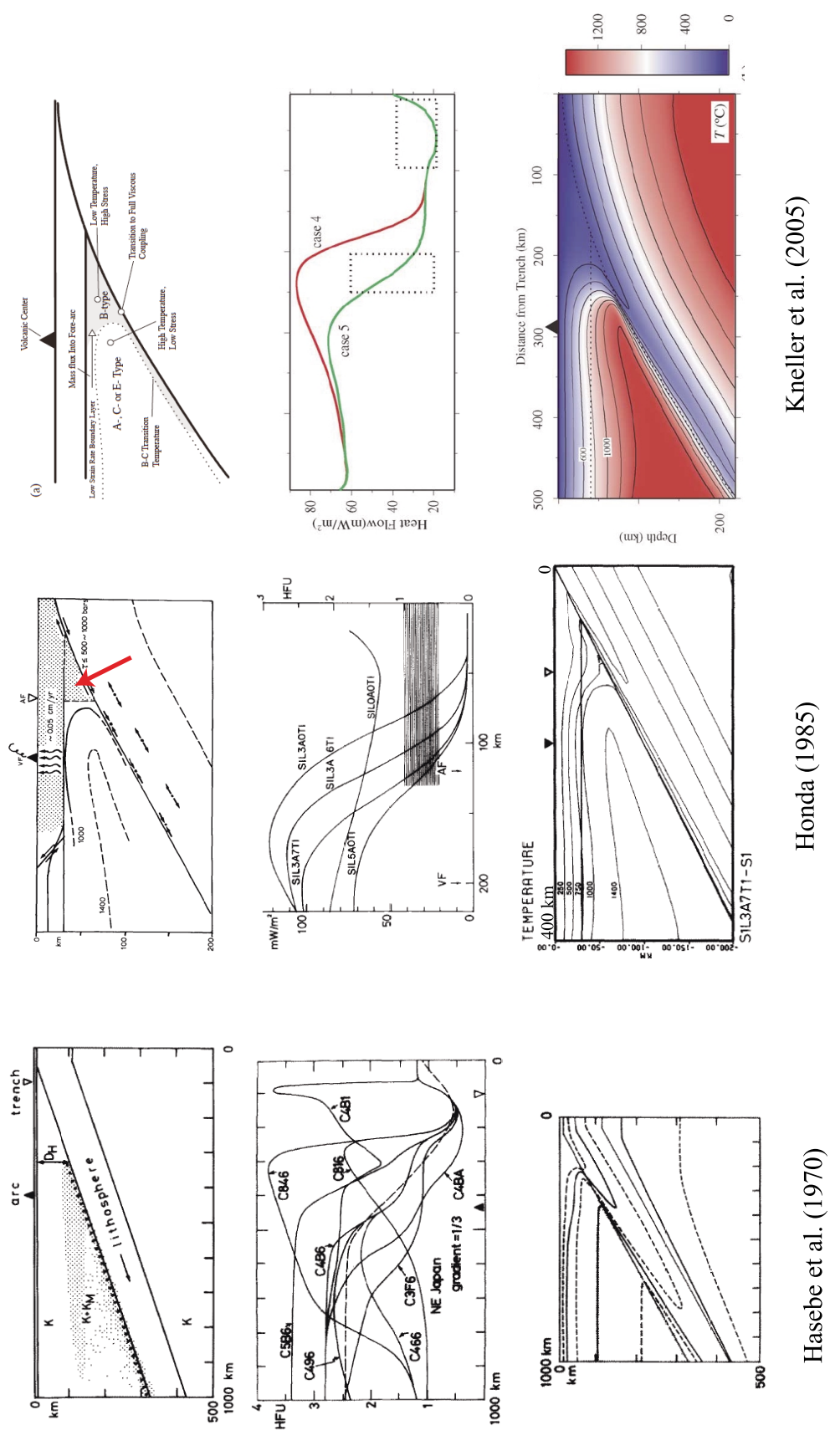

Fig. 3. Chronological developments of the subduction zone models under northeast Japan. The left-hand, the middle and the right-hand columns of the figure are the models presented by Hasebe *et al.* (1970), Honda (1985) and Kneller *et al.* (2005), respectively. The top, the middle and the bottom figures of each column show the concept of the model, the heat flow distribution obtained for various model parameters, and the results, respectively. Left: Reprinted from figures 4, 6, and 9 of *Tectonophysics, 10*, Hasebe, K., N. Fujii, and S. Uyeda, Thermal processes under island arcs, 335–355, Copyright 1970, with permission from Elsevier. Middle: Reprinted from figures 7, 13, and 19 of *Tectonophysics, 112*, Honda, S., Thermal structure beneath Tohoku, northeast Japan—A case study for understanding the detailed thermal structure of the subduction zone, 69–102, Copyright 1985, with permission from Elsevier. Right: Reprinted from figures 8 and 9 of *Earth Planet. Sci. Lett., 237*, Kneller, E. A., P. E. van Keken, S. Karato, and J. Park, B-type olivine fabric in the mantle wedge: insights from high-resolution non-Newtonian subduction zone models, 781–797, Copyright 2005, with permission from Elsevier.

doi:10.5047/meep.2017.00502.0035

front, which roughly corresponds to the depth limit of the existence of the thrust-type earthquakes, is around 60 km, which is the preferred value of D_H of Hasebe *et al*. (1970).

The model presented by Kneller *et al*. (2005) (right-hand column of Fig. 3) included sophisticated rheology; that is, diffusion creep and dislocation creep (e.g., Karato and Wu, 1993). Special attention was paid to the coupling between the mantle wedge and the subducting slab. Kneller *et al*. (2005) found that full decoupling above 40 km, and partial coupling from 40 km to 70 km, could explain the heat flow distribution and the results of seismic tomography. "Decoupling" in their study meant that the speed of the mantle wedge in contact with the subducting slab was smaller than that of the slab. Full decoupling meant that it was 0. They also concluded that the B-type fabric of olivine (Jung and Karato, 2001) exists in the fore-arc mantle. Such a fabric may explain the seismic anisotropy which shows the trench-parallel fast axes in the fore-arc region (Nakajima *et al*., 2006).

The studies mentioned above mainly focused on the two-dimensional across-arc feature of the subduction zone and did not consider seriously the spatial and temporal variation of the subduction zone. This was because of the paucity of observations relating to the spatial and temporal variation of the subduction zone and the lack of powerful computational tools and methods at that time. Today, this is no longer the case, and, to a certain degree, we can compare the results of numerical simulations with the available observations.

In the following sections, we focus on the thermomechanical modeling of subduction zones mainly based on our studies. One of the important missing topics in this review is the role played by fluids, and some discussion of this is given in Appendix B.

2. Issues Related to the Subduction Zone around the Japanese Islands

Figure 4 shows the P-wave seismic tomography model NECCES_P1NT (Obayashi *et al*., 2012). Major prominent features are the fast-velocity anomaly extending from the trench to the back-arc, and the broad high-speed anomaly around the transition zone. These are usually attributed to the subduction of the slab and the stagnation of the slab caused by the interaction between the cold slab and phase transitions (Fukao *et al*., 2009). We also recognize a slow-velocity anomaly around a depth of 400 km under the Pacific plate, which is considered to be mainly a temperature anomaly (Obayashi *et al*., 2006). At a local scale of seismic tomography studies of northeast Japan, a close correlation between the slow-velocity anomaly and volcano distribution has been recognized (Tamura *et al*., 2002; Hasegawa and Nakajima, 2004: see later sections).

The features mentioned above may be linked to the mantle processes there. Thus, in this review, and based on our research, we discuss: (1) the existence of small-scale convection within the mantle wedge under northeast Japan and Izu-Bonin (Fig. 4, Region A); (2) the flow around the junction; (3) the existence of a hot anomaly in the sub-slab mantle under the Pacific plate (Fig. 4, Region B); and (4) the nature of the western edge of the stagnant slab (Region C), and the slab gap (Fig. 4; Region c).

3. Small-scale Convection (SSC) within the Mantle Wedge

In northeast Japan, Tamura *et al*. (2002) grouped the distribution of recent volcanoes into several clusters elongated nearly parallel to the direction of the convergence (Fig. 5(a)), and found a good correlation between them and geophysical observations such as the low-velocity anomaly (Fig. 5(b): Hasegawa and Nakajima (2004)) in the mantle wedge and the Bouguer anomalies.

Tamura *et al*. (2002) regarded these features as the surface manifestation of the finger-like hot mantle in the mantle wedge and called them "hot fingers".

As discussed below, Honda and Yoshida (2005a) examined the past distribution of volcanoes and recognized two characteristics of their temporal and spatial changes; namely, (1) the flip-flopping of fingers (the description "fingers" is also used for the pattern of volcano distribution), and (2) the migration of volcanic activity from the back-arc side to the trench side. Flip-flopping means that an area of inactivity becomes active, later, or vice-versa.

Figures 6(a) and 6(b) show the past distribution of volcanoes estimated from the volcanic rocks and the related strata from 10 Ma to 5 Ma and from 5 Ma to the present, respectively. Figure 6(c) shows the ages and the longitudinal positions of the volcanoes in the region enclosed by dotted lines in Figs. 6(a) and 6(b), where a prominent flip-flopping pattern of the volcano distribution is recognized. From Fig. 6(c), we recognize the migration of volcanic activity from the back-arc to the trench, especially during $\sim$5 Ma to the present. Similar alignments and age distribution of seamount chains are also recognized in the Izu-Bonin region (Fig. 6(d)). Differences between the northeast Japan arc and the Izu-Bonin arc are that the seamount chains in the Izu-Bonin arc are not active now and they align obliquely to the direction of the present convergence plate velocity (Fig. 6(d)). These characteristics may constrain the models to explain the origin of the finger-like pattern of volcano distribution.

If the temporal and spatial change of the distribution of past volcanoes reflects the past pattern of hot fingers, the time-scale related to the fingers will be of the order of a few million years. This suggests that mantle processes play a significant role, rather than those related to water and/or volatiles, which affect the melting processes also, since the time-scale of their movements is considered to be short because of their extremely low viscosity.

Recognizing that the finger pattern is similar to that of the roll pattern of the SSC under the oceanic lithosphere (Richter and Parsons, 1975), Honda and his collaborators studied the SSC driven by the thermal buoyancy in the mantle wedge (Honda *et al*. (2002); Honda and Saito (2003) and those described below).

Figure 7 shows the conceptual view of the SSC model. The flow induced by the subducting slab plays a role as a large-scale flow in the case of the SSC under the oceanic

doi:10.5047/meep.2017.00502.0035

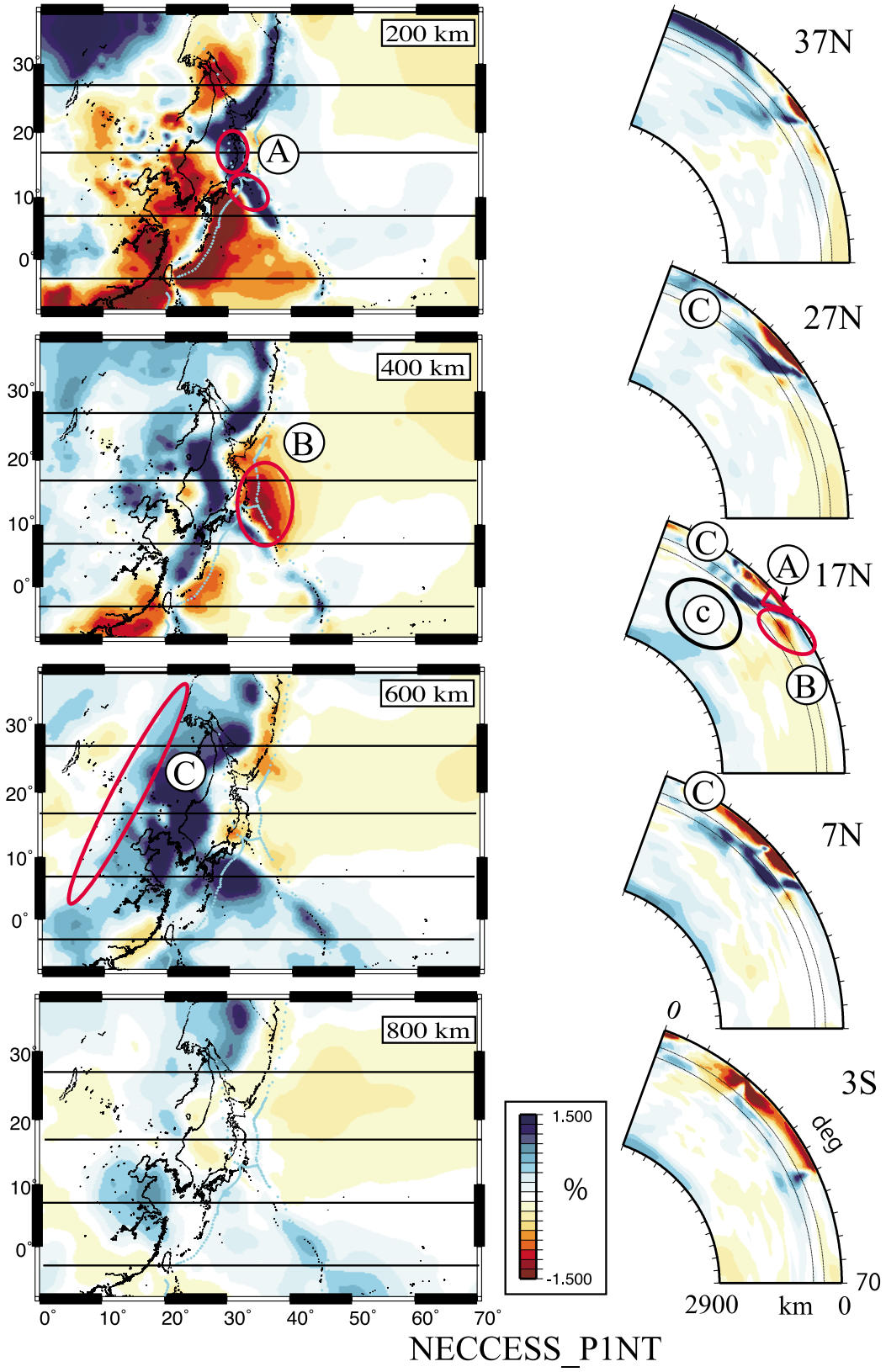

Fig. 4. The *P*-wave seismic tomography model NECCES_P1NT (Obayashi *et al*., 2012). The left-hand column shows the plan view at 200, 400, 600 and 800 km depths. These are constructed by the Mercator projection whose pole is that of the relative plate motion between the Eurasia plate and the Pacific plate (NUVEL1A: DeMets *et al*., 1994). The right-hand column shows the cross-sections at 37N, 27N, 17N, 7N and 3S.

doi:10.5047/meep.2017.00502.0035

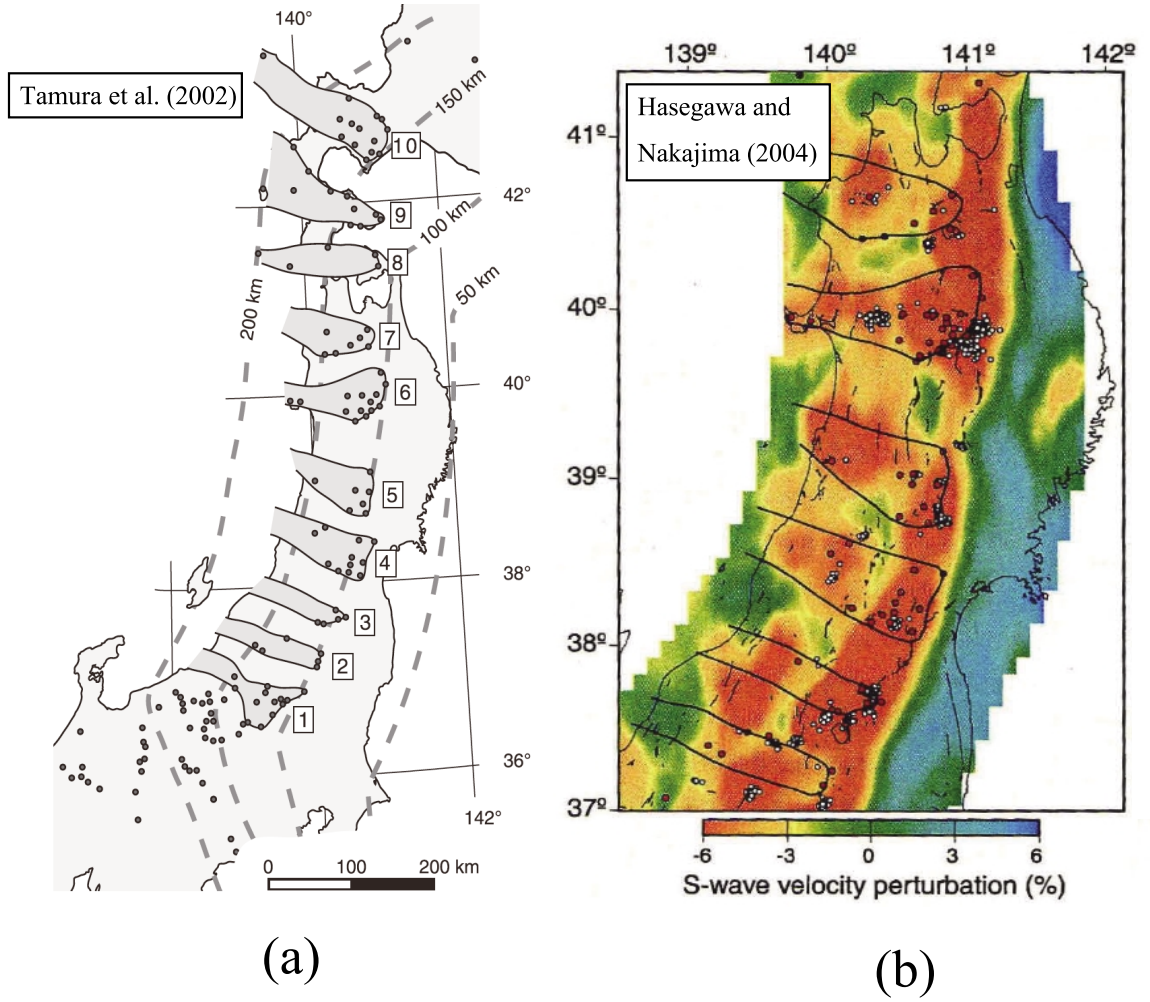

Fig. 5. (a) Distribution of recent volcanoes (black dots) and their groupings (hot fingers: thin lines) from Tamura *et al*. (2002). Dashed lines show the iso-depth contours of the Wadati-Benioff zone. Reprinted from figure 9 of *Earth Planet. Sci. Lett*., *197*, Tamura, Y., Y. Tatsumi, D. Zhao, Y. Kido, and H. Shukuno, Hot fingers in the mantle wedge: new insights into magma genesis in subduction zones, 105–116, Copyright 2002, with permission from Elsevier. (b) Correlation between the hot fingers (thin lines) and the slowest *S*-wave perturbation in the mantle wedge from Hasegawa and Nakajima (2004).

lithosphere (Richter and Parsons, 1975). The SSC occurs within the mantle wedge, if there is a low-viscosity zone above the subducting slab (we call this LVW, "low-viscosity wedge", hereafter). Such an LVW may be produced by the water released from the subducting slab and/or the melt there. However, actually, we determined the size, shape and the viscosity of the LVW so that the results can explain the observed temporal and spatial pattern of the volcano distribution rather than that it was obtained self-consistently based on the modeling of fluid processes and its effects on the rheology. We think that this approach is a kind of inversion similar to, for example, the analysis of earthquake source mechanisms based on the observed seismic waves without a physical modeling of fault movements. In Appendix B, we discuss some of these points. The pattern of the resultant SSC is expected to be roll-like and their axes align in the direction of large-scale flow, that is, that of the plate velocity.

Using 2D models, Gerya and Yuen (2003) proposed an SSC driven by chemical buoyancy in the mantle wedge and proposed that "hot fingers" are actually "cold fingers". This occurs since the chemically buoyant plumes, caused by water dehydrated from the slab, rise from the upper part of the subducting slab where the temperature is low (also see Honda *et al*. (2010)). Except for the difference in the origin of the buoyancy, both the thermal and chemical SSC have similar characteristics. For example, both models require the LVW of $O(10^{18})$ Pa·s for the occurrence of gravitational instability (e.g., Honda and Yoshida, 2005a; Zhu *et al*., 2009). Thus, we focus on the thermal SSC which has been studied mainly by us.

Figure 8 shows the general outline of the numerical model, although the details may be different for individual works. The geometry and the speed of the subducting slab are given *a priori*. The gray zones show the conductive (rigid) layer of Honda (1985). In Fig. 8, the vertical cross-section of the LVW is shown and extends parallel to the right wall. The geometry of the LVW is usually fixed in space, and the viscosity is decreased by multiplying by a factor less than 1 the pressure- and temperature-dependent or region-dependent viscosity.

doi:10.5047/meep.2017.00502.0035

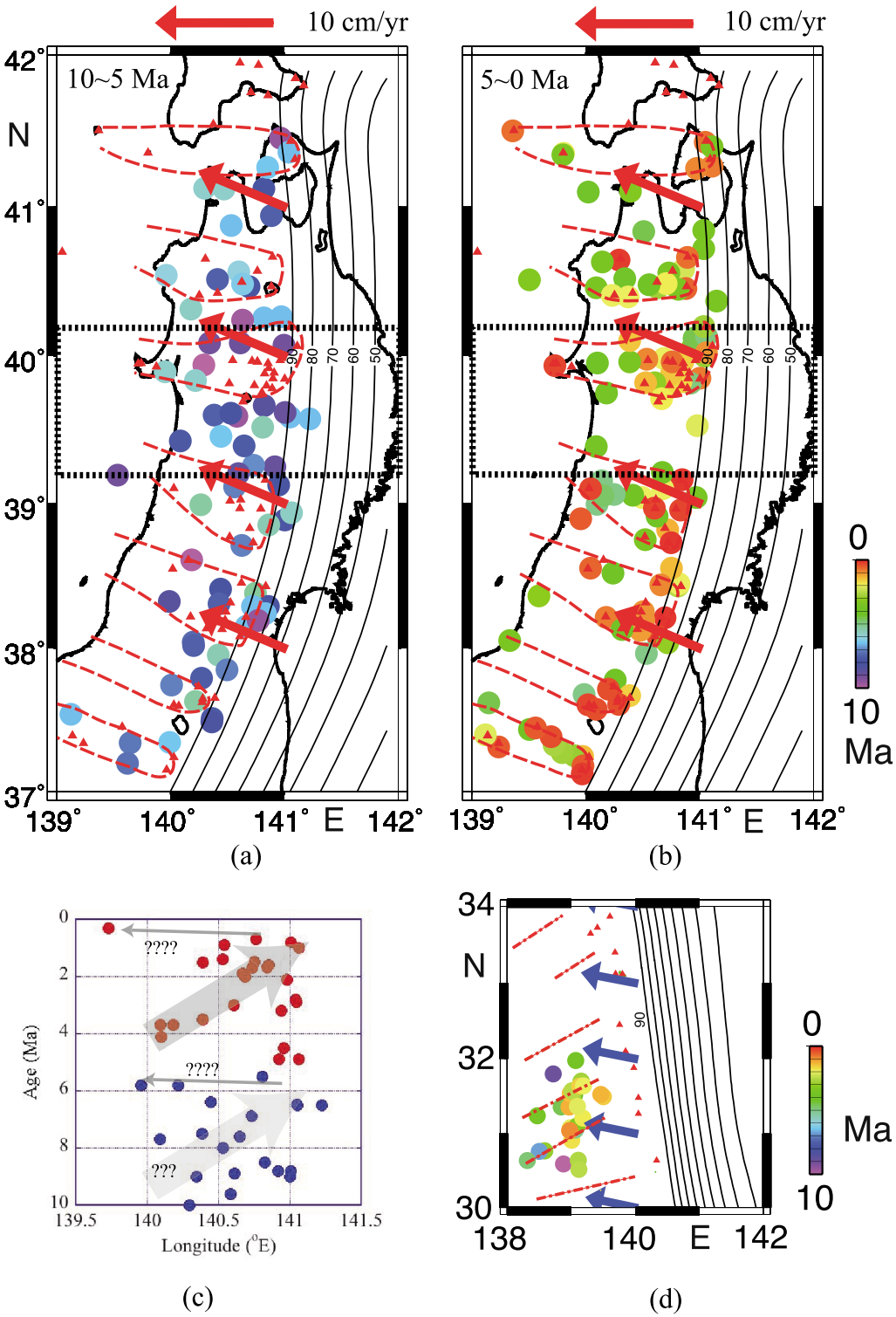

Fig. 6. (a) Distribution and age of rocks and strata related to a volcanic origin from 10 to 5 Ma (Data from Honda and Yoshida (2005a)). Red triangles show the positions of recent volcanoes. Dashed lines show the hot fingers (Tamura *et al*., 2002) and thin lines show the iso-depth contours of the upper plane of the subducting Pacific plate up to a depth of 90 km (CAMP Standard Model Version 1: Hashimoto *et al*. (2004)). The arrows show the relative motion between the Pacific plate and the North America plate (Seno and Sakurai, 1996). (b) Distribution and age of rocks and strata related to a volcanic origin from 5 to 0 Ma (Data from Honda and Yoshida (2005a)). See the caption of (a) for further details. (c) Age and longitudinal position of rocks and strata related to a volcanic origin in the region enclosed by the dotted lines in (a) and (b). Colors show the ages from 10 to 5 Ma (blue) and 5 to 0 Ma (red), which roughly corresponds to the distribution in the southern part and the northern part of the region enclosed by dotted lines in (a) and (b), respectively. Data from Honda and Yoshida (2005a). (d) Distribution and age of rocks from 10 to 0 Ma (Data from Honda *et al*. (2007b)) in the Izu-Bonin region. Blue arrows show the relative motion between the Pacific plate and the Philippine Sea plate (Seno *et al*., 1993). See the caption of (a) for further details.

doi:10.5047/meep.2017.00502.0035

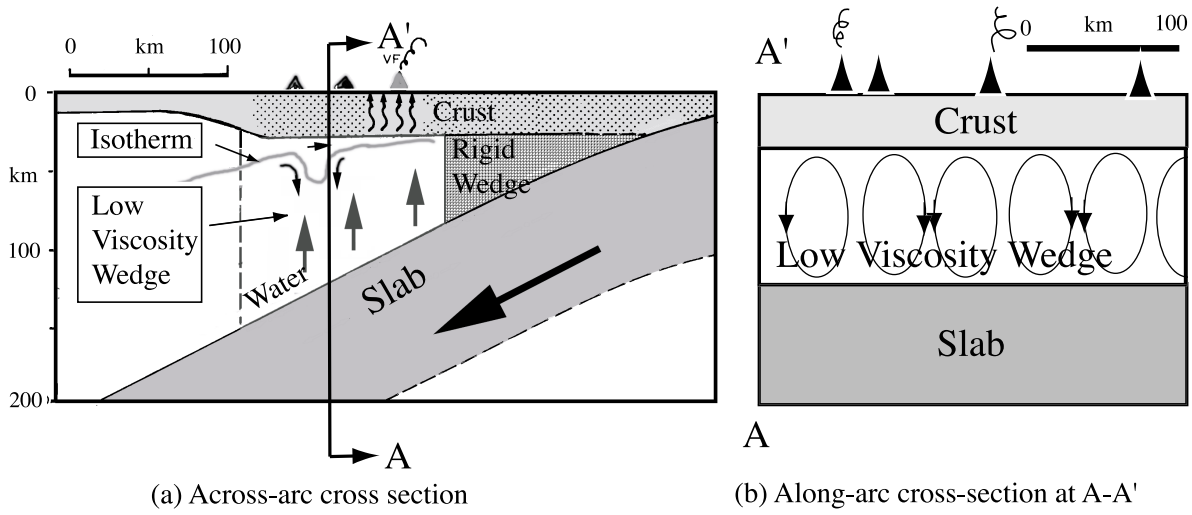

Fig. 7. Sketch of the small-scale convection (SSC) model after Honda *et al*. (2007b). (a) A cross-section perpendicular to the trench. An SSC may occur if there is a low-viscosity wedge (LVW) caused by water released from the subducting slab and/or a melt. (b) Cross-section along the trench. The SSC may have a roll-like structure whose axes align in the direction of the convergence. In response to the pattern of the SSC, volcanoes may be distributed like fingers. Reprinted from figure 3 of *Island Arc*, *16*, Honda, S., T. Yoshida, and K. Aoike, Spatial and temporal evolution of arc volcanism in the northeast and Izu-Bonin arcs: Evidence of small-scale convection under the island arc? 214–223, Copyright 2007, with permission from John Wiley & Sons.

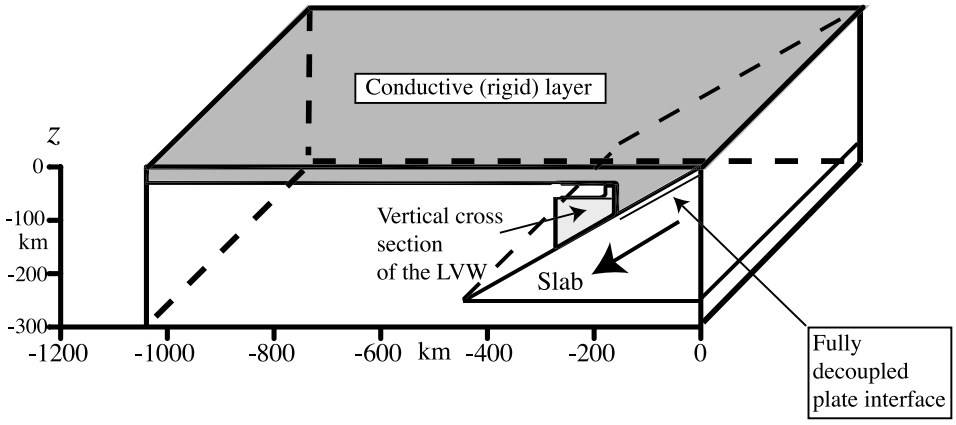

Fig. 8. Geometry of the SSC model (Modified from Honda *et al*. (2007b)). Gray zones show the rigid regions and "LVW" is the low-viscosity wedge where the viscosity is lowered. The movement of the slab is kinematically applied. Modified from figure A1 of *Island Arc*, *16*, Honda, S., T. Yoshida, and K. Aoike, Spatial and temporal evolution of arc volcanism in the northeast and Izu-Bonin arcs: Evidence of small-scale convection under the island arc? 214–223, Copyright 2007, with permission from John Wiley & Sons.

Figure 9 shows a typical case of a flip-flopping of fingers; that is, the exchange of high- and low-temperature regions with time (Honda and Yoshida, 2005a). This flip-flopping starts to occur from the back-arc side and propagates toward the trench side. This pattern change is qualitatively similar to that of the past volcano distribution as described before; that is, (1) the flip-flopping pattern, and (2) the migration of volcanic activity from the back-arc side to the trench side. However, it is found to be rather difficult to achieve quantitative agreement, especially between the speed of migration of volcanic activities and that of the pattern change associated with the flip-flopping of the modeled temperature field. In northeast Japan, observations suggest that it is ∼2 cm/yr (see Fig. 6(c)) which is significantly smaller than that of the convergence (∼10 cm/yr). Although we could obtain a model which shows a quantitative agreement with the observations by assuming a fairly complex structure of the LVW (Honda, 2011), results of simple models show that the predicted migration speed is generally comparable to the speed of the convergence.

We also studied the effects of oblique subduction, the along-arc movement of a part of the overlying plate, and the dip angle of the subducting slab in order to apply the SSC model to the Izu-Bonin arc where the Pacific plate subducts obliquely under the Philippine Sea plate (Fig. 10; Honda and Yoshida, 2005b; Honda *et al*., 2007b).

We found that; (1) even when the slab subducts obliquely, the axes of the resultant roll-like SSC are normal to the strike of the trench (Fig. 10(b)) similar to the case where the convergence velocity is normal to the strike of the trench (Fig. 10(a)), (2) the SSC aligns obliquely, if the overlying plate is moving toward the along-arc direction (Fig. 10(c));

doi:10.5047/meep.2017.00502.0035

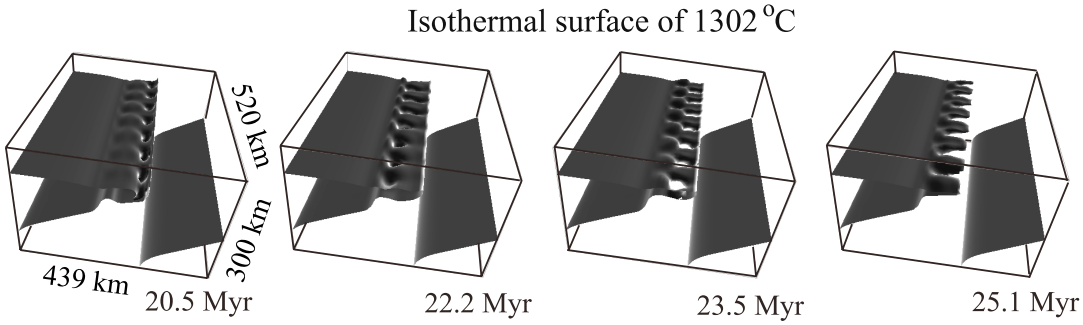

Fig. 9. Iso-temperature surface of 1302°C obtained from the SSC model (Modified from Honda *et al*. (2005a)). The slab subducts from the top right. Age shows the time after the start of the run. Flip-flopping is clear, especially on the far side of the model.

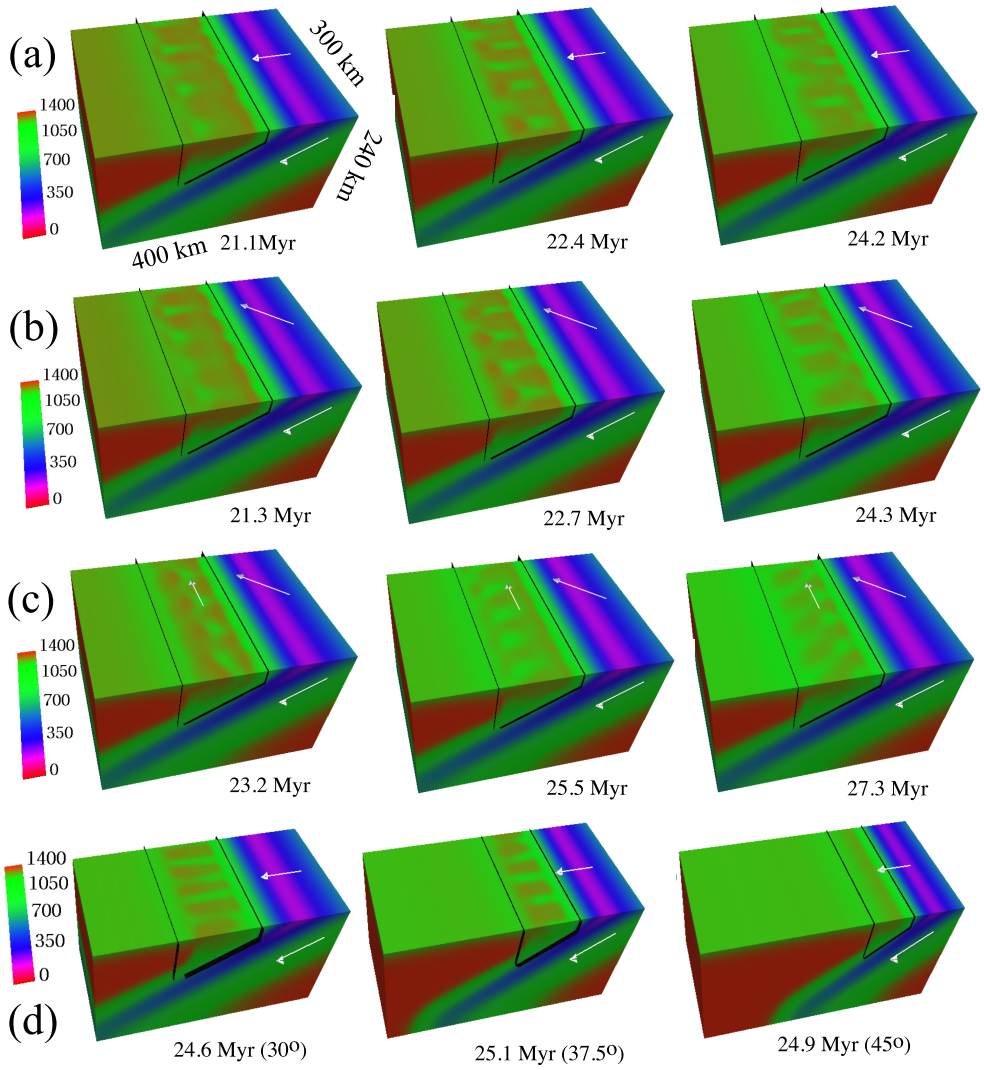

Fig. 10. Various effects on the SSC (Honda *et al*., 2007b). The velocity component normal to the trench is set to 2.50 cm/yr and the greatest depth of the LVW is 150 km for all models. The thin black lines show the region of the LVW. White arrows show the given plate velocities. Age shows the time after the start of the run. (a) The direction of the subduction is normal to the trench (plate boundary). (b) The direction of subduction is oblique to the trench. (c) The direction of subduction is oblique to the trench. The top surface of the LVW moves toward the direction of the oblique direction of the subduction. (d) Change of the dip angle of the subducting plate. Numbers in brackets are the dip angles of each model. Reprinted from figure 4 of *Island Arc*, *16*, Honda, S., T. Yoshida, and K. Aoike, Spatial and temporal evolution of arc volcanism in the northeast and Izu-Bonin arcs: Evidence of small-scale convection under the island arc? 214–223, Copyright 2007, with permission from John Wiley & Sons.

doi:10.5047/meep.2017.00502.0035

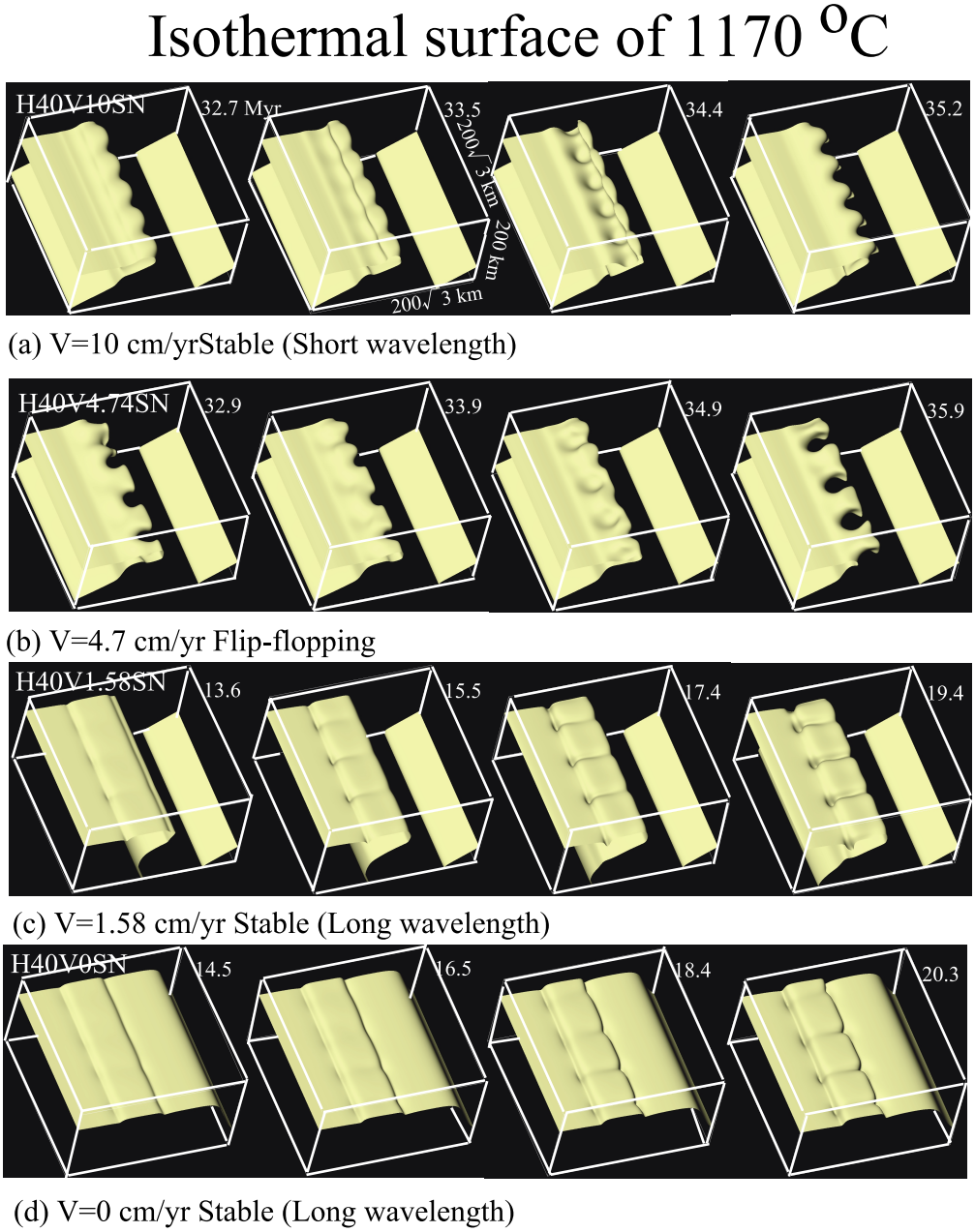

Fig. 11. Figures showing the transition from the stable short-wave instability, flip-flopping and the stable long-wave instability. Results are from Honda (2011). The 3D surface shows the isothermal surface (1170°C) and the region covers $200\sqrt{3}$ km $\times 200\sqrt{3}$ km $\times 200$ km. The speed of the subduction gradually changes from the top to the bottom. Flip-flopping is recognized in the second row. The age (Myr), shown in the right corner of each figure, indicates the time after the start of the run.

(3) as the dip angle of the subducting plate becomes large, the SSC disappears (Fig. 10(d)). In these models, the greatest depth of the LVW was kept the same (150 km). From these results and geologic observations, Honda *et al*. (2007b) inferred that the oblique seamount chains in the back-arc of the Izu-Bonin arc (Fig. 6(d)), which may be the fingers, were produced by along-arc movement of the back-arc lithosphere after the cessation of SSC activity, and they became inactive because of the increase of the dip angle of the subducting Pacific plate (van der Hilst and Seno, 1993). Honda (2008) studied the effects on the SSC of trench retreat and advance and found that they did not significantly affect the results providing the relative velocity is kept the same.

Later studies using a simple trapezoidal geometry of the LVW indicate that many cases show a rather stable pattern of the fingers (Fig. 11; Honda, 2011). Honda (2011) concluded that the flip-flopping pattern is a transitional state from the state dominated by the long-wavelength instability characterized by the greatest depth of the trapezoidal LVW to that dominated by the short-wavelength instability characterized by the most shallow depth of the trapezoidal LVW (Fig. 11).

Since we can hardly know the past history of the presently active region, there is still a possibility that the pattern of fingers on northeast Japan is stable (see Kondo *et al*. (1998)).

doi:10.5047/meep.2017.00502.0035

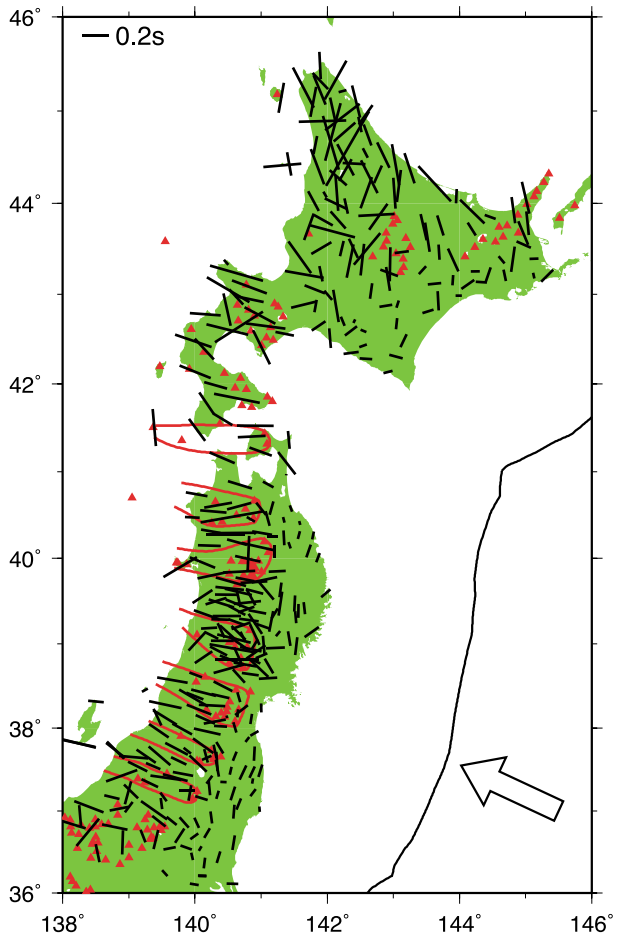

Fig. 12. *S*-wave polarization anisotropy obtained by Nakajima *et al*. (2006). The direction and the length of the black bars indicate the fast direction and the travel-time difference between the *S*-waves oscillating in the fastest polarization direction and those oscillating in the slowest polarization direction. The arrow indicates the direction of the relative plate motion between the North America plate and the Pacific plate, in the vicinity, i.e., N65W (DeMets *et al*., 1994).

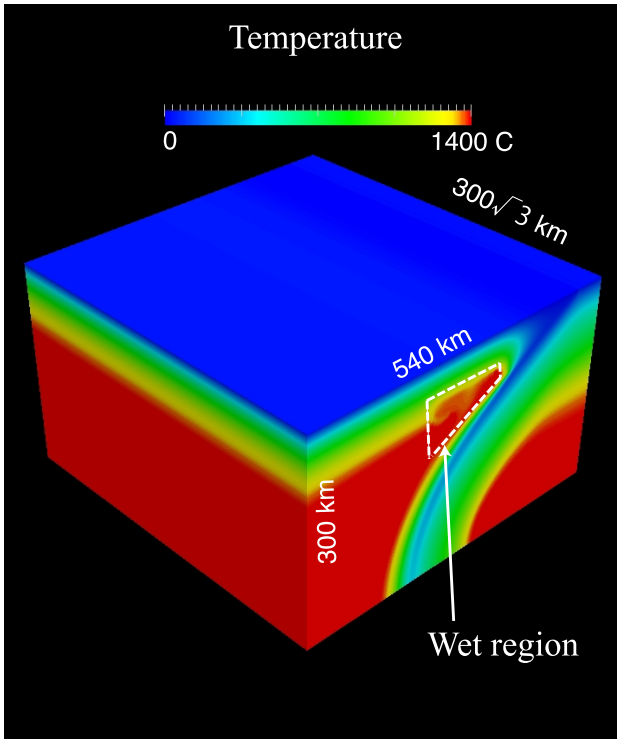

Fig. 13. A result of a model presented by Morishige and Honda (2013). We use the wet rheology of olivine in the region shown by the dashed lines ("Wet region"). Outside this region, we use the dry olivine rheology.

However, such a stable pattern may not be able to explain the migration of volcano distribution from the back-arc to the trench. Thus, to constrain the model, it is necessary to confirm the above-mentioned two characteristics of the past volcano distribution. This may be achieved by studying the other arcs with comparable details as those of northeast Japan.

The seismic anisotropy caused by the lattice-preferred orientation of the minerals may become the clue to constrain the mantle flow. Figure 12 shows the results obtained by Nakajima *et al*. (2006) for the shear wave polarization anisotropy. The direction and the length of the bars show the fast direction and the magnitude of the delay time between the *S*-wave oscillating parallel to the fast polarization direction and that oscillating parallel to the slowest polarization direction.

The most prominent feature of these results is that the fast direction of the region behind the volcanic front aligns almost normal to the strike of the trench, while that of the fore-arc region aligns in the trench-parallel direction. The latter observation may be explained by a change in the fabric of the olivine (Kneller *et al*., 2005), rather than that of the mantle flow. We shall pay attention to the anisotropy of the former region in the following discussions, since our models did not calculate the flow field under the fore-arc region (we assumed that that part was rigid).

Morishige and Honda (2011) studied the SSC using wet and dry olivine rheology and estimated the resultant seismic anisotropy. In their models, the LVW is the "wet region" where the wet olivine rheology is used (Fig. 13).

Figure 14 shows an example of the estimated fast direction of the *P*-wave anisotropy projected on the 75-km-depth plane (Fig. 14(a)) and along the cross-sections where the upwelling or downwelling is dominant (Figs. 14(b) and 14(c)). The temperature anomaly, i.e., the deviation from the horizontally averaged temperature, is also shown in Fig. 14. The overall pattern of the anisotropy is the fast direction parallel to that of the convergence velocity. However, its magnitude becomes smaller than the case without SSC (Fig. 14(d)), which is similar to the case of SSC under the oceanic lithosphere (van Hunen and Čadek, 2009). It is, therefore, necessary to determine the 3D anisotropy pattern to constrain the flow within the mantle wedge.

Recently, Morishige (2015) proposed a different type of model of the origin of the finger-like pattern. In his model, he assumed a thin low viscosity layer (LVL) above the top surface of the subducting slab just below the fully-decoupled plate interface. In 3D cases, the flow penetrating into the LVL changes along-arc because of the effect of the temperature-dependent viscosity. The warmer, and hence,

doi:10.5047/meep.2017.00502.0035

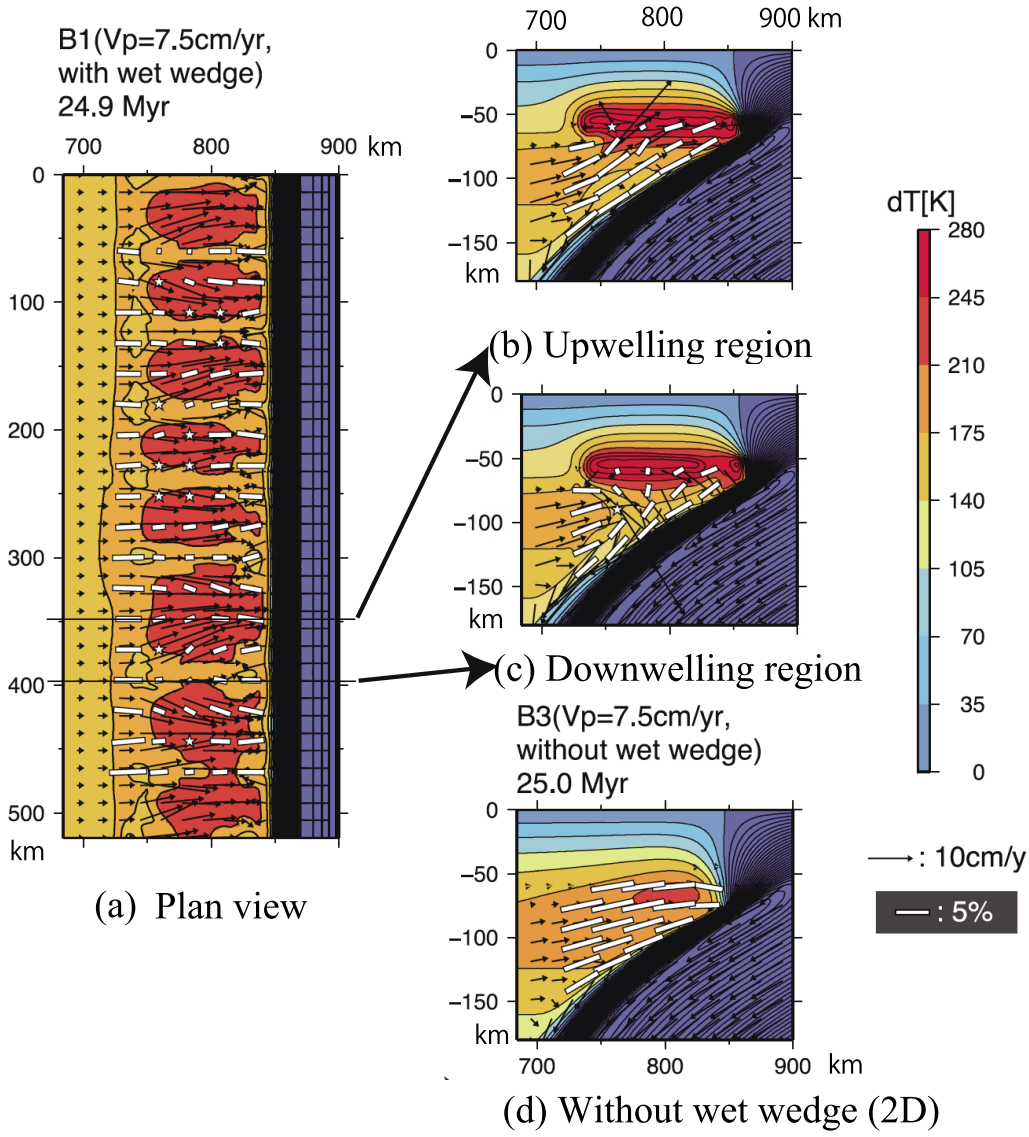

Fig. 14. An example of results from Morishige and Honda (2013). Age shows the time after the start of the run. (a) The velocity (black arrows) and the fast direction of the P-wave seismic anisotropy projected on the 75-km-depth plane (white bars). In addition, the temperature deviation from the horizontally-averaged temperature (color) is shown. (b) The same as (a) for the vertical cross-section, where the upwelling flow dominates. (c) The same as (a) for the vertical cross-section where the downwelling flow dominates. (d) The same as (a) for the 2D models without the SSC. This is the vertical cross-section.

less viscous mantle wedge material can penetrate into the LVL easier than the colder, more viscous, because the latter is more coupled to the downward movement of the subducting slab. Thus, there occurs an imbalance of the mass flux between the warmer region and the colder region, which is accommodated by the along-arc flow in the LVL. One merit of his model over the SSC models is that it does not require a large LVW in the mantle wedge, whose origin is controversial. It is found that the obtained finger-like structure is relatively stable in his model (M. Morishige, pers. comm., 2015), and it develops from the trench side.

4. Large-scale 3D Flow around the Subduction Zone

Along-arc variations of plate scale, say, $O(1000$ km) are expected to induce significant 3D flows. Honda (2009) studied the flow around the slab edge, similarly to that at the junction between the Kamchatka arc and the Aleutian arc (Fig. 15(a)). This case is considered to be an extreme case of a trench-trench junction. Peyton *et al.* (2001) and Long and Silver (2008) proposed the existence of a flow which is sub-parallel to the along-arc direction in the sub-slab mantle. This type of flow may explain the trench-parallel seismic anisotropy in the sub-slab mantle (Long and Silver, 2008). Honda (2009) studied the cases with a small trench retreat (the first row of Fig. 15(b)), a significant trench retreat (the second row of Fig. 15(b)), a significant trench advance (the third row of Fig. 15(b)), and a small trench retreat coupled with a hot anomaly in the sub-slab mantle under the subducting slab (the fourth row of Fig. 15(b)). He found that the trench-parallel flow in the sub-slab mantle is generally weak and suggested that the hot or buoyant anomaly in the

doi:10.5047/meep.2017.00502.0035

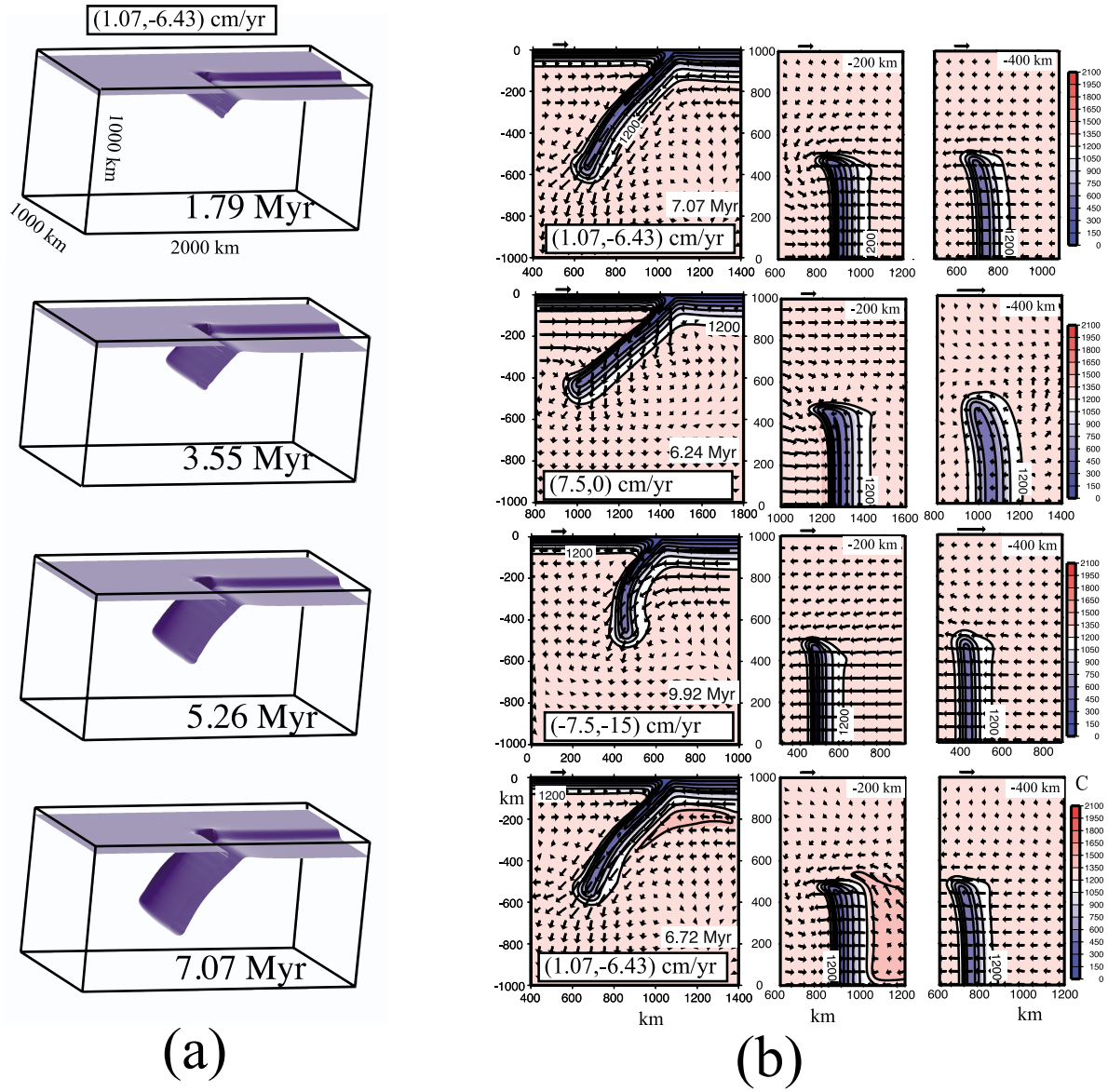

Fig. 15. (a) Temporal evolution of the subducting slab around the edge (Honda, 2009). The figure shows an isothermal surface of 1000°C. The region covers 1000 km × 2000 km × 1000 km. The numbers in the box show the speed of the left plate and the right plate. Age shows the time after the start of the run. (b) Vertical and horizontal cross sections of temperature and the flow (results arranged from Honda (2009)). The position of the vertical cross-section (first column) is the center of the subducting slab. Positions of the horizontal cross-section (second and third columns) are depths of 200 km and 400 km. The numbers in the boxes show the speed of the left plate and the right plate. The age shows the time after the start of the run. Reprinted from figures 3, 4, 5, 6, and 8 of *Earth Planet. Sci. Lett.*, *277*, Honda, S., Numerical simulations of mantle flow around slab edges, 112–122, Copyright 2009, with permission from Elsevier.

sub-slab mantle may produce the proposed flow.

Morishige and Honda (2013) studied the flow around the junction between the northeast Japan arc and the Kurile arc (Figs. 16(a), (b), (c)). They showed that there is a general consistency between the seismic anisotropy estimated from the modeling (Fig. 16(c)) and that observed (Fig. 12). That is, the fast direction of the *S*-wave polarization anisotropy under the back-arc is nearly normal to the strike of the arc even in the region of oblique subduction (Fig. 16(c)). The distribution of the fast direction is somewhat disturbed in the back-arc side near the trench. This occurs probably because that area corresponds to the turning point of the flow from the trench normal at a shallow depth to the direction of the convergence above the subducting slab (see the particle trajectory in Fig. 16(b)). This trench-normal pattern was also shown by Kneller and van Keken (2008) using a model having a fixed geometry of the slab and the speed of the subduction. Morishige and Honda (2013) also showed that the angle of the subduction under northeast Japan is smaller than that under Kurile, and such a difference may result in a different mode of slab stagnation (Fig. 4). Torii and Yoshioka (2007) showed that the stagnation occurs with decreasing dip angle. This difference of subduction angle is explained by a simple 2D torque balance model (Stevenson and Turner, 1977) on the cross-section normal to the trench (Morishige and Honda, 2013). Under northern Okhotsk (Kamchatka),

doi:10.5047/meep.2017.00502.0035

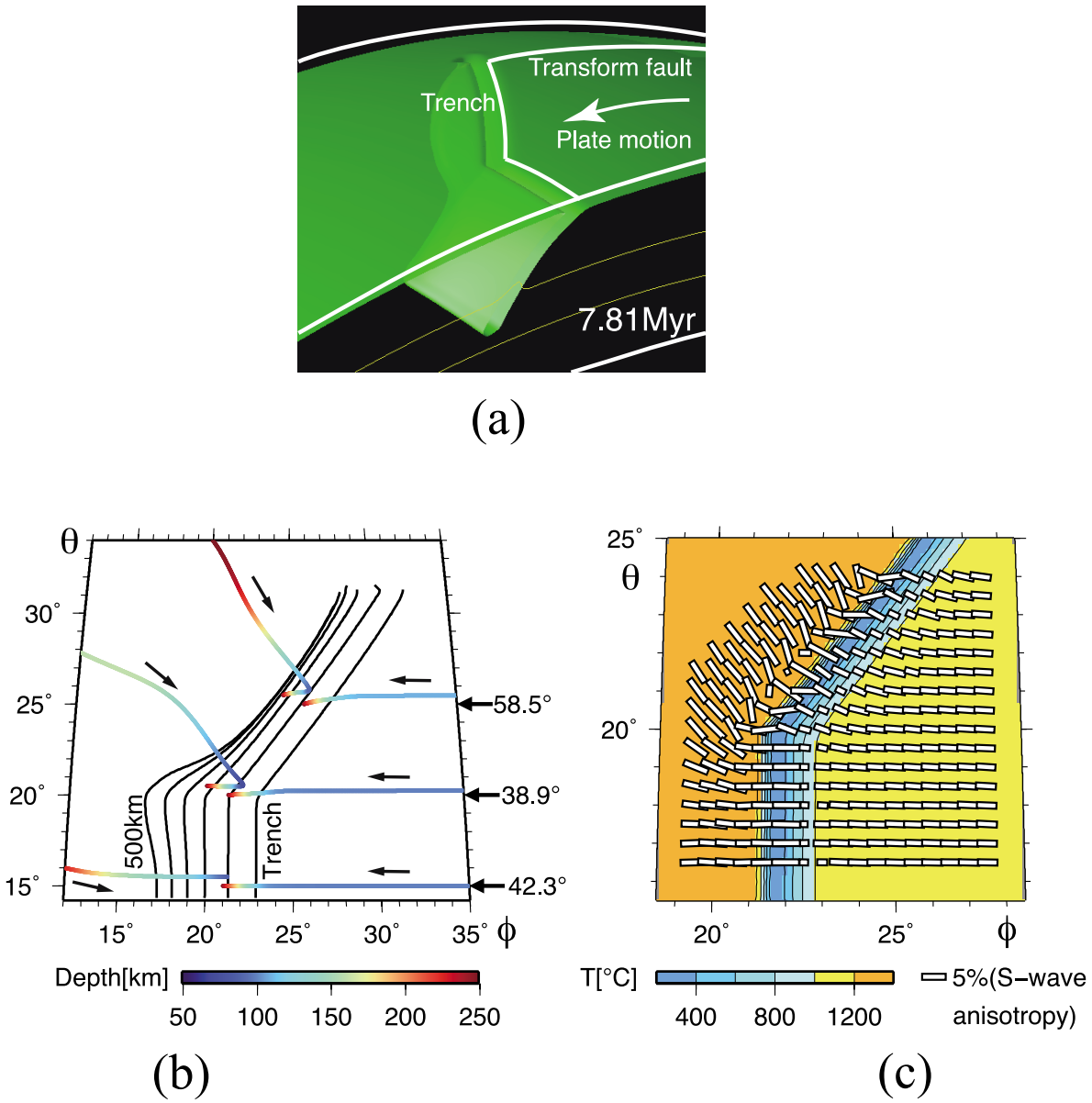

Fig. 16. (a) A 3D presentation of an isothermal surface (1000°C) from Morishige and Honda (2013). The age shows the time after the start of the run. (b) Plan view of the depth contour of the isothermal surface (1000°C). Blue lines show the particle trajectories. (c) Fast direction of the *S*-wave polarization anisotropy projected on the plane at a 100-km depth (white bars). The temperature distribution at a depth of 100 km is shown in color scale. Reprinted from figures 3 and 4 of *Earth Planet. Sci. Lett.*, *365*, Morishige, M. and S. Honda, Mantle flow and deformation of subducting slab at a plate junction, 132–142, Copyright 2013, with permission from Elsevier.

where the angle of subduction is larger, the slab appears to penetrate through the lower mantle. Meanwhile the slab below northeast Japan, where the dip angle is smaller, shows a prominent stagnation in the transition zone. There, the angle of the subduction at the junction is smallest and the length of the stagnant slab is longer (Fig. 16(b)). Seismic tomography shows that the stagnation of the slab is more evident in the direction extending from the junction. This is consistent with our results. These results show that the shape of the plate boundary affects the dynamics of the subducting slab. We will show later that this point is related to the last topic.

Recently, Wada *et al*. (2015) presented a 3D thermomechanical model of subduction around this area. Their model assumed a seismologically-inferred slab in which the flow velocity is given, while our model only assumed the plate velocity on the top surface and along the shallow plate boundary. They showed the presence of a relatively cold region near the junction, which was recognized in our model also.

5. Hot Anomaly in the Sub-slab Mantle

Obayashi *et al*. (2006) analyzed the slow-velocity anomaly, which correlates well with the 410-km seismic discontinuity, in the sub-slab mantle under the Pacific plate (Fig. 4, Region B) and concluded that it is mainly a high-temperature anomaly of ∼200 K. Following seismological

doi:10.5047/meep.2017.00502.0035

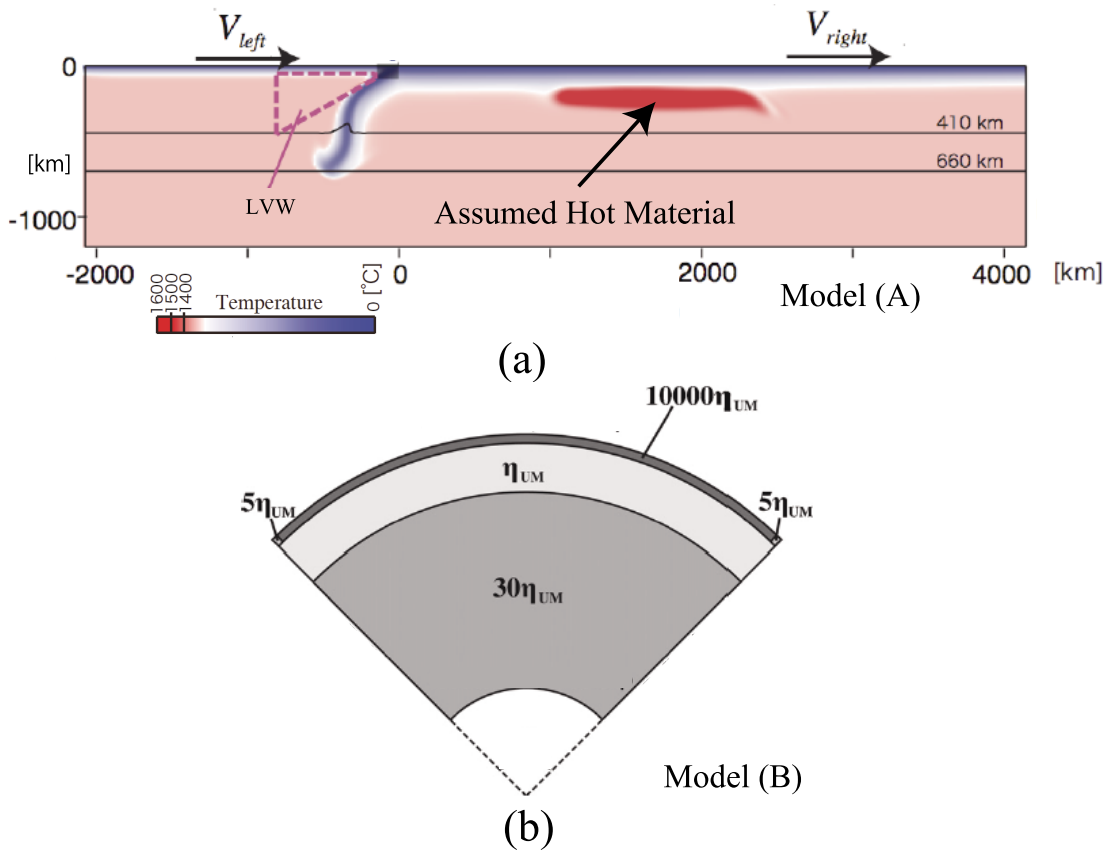

Fig. 17. (a) Geometry of the model (A) used to study the case of a hot anomaly carried far from the subduction zone (Modified from Morishige *et al.* (2010)). Plate velocities on the top surface and the shallow plate boundary are imposed. The hot anomaly is set into the model as an initial condition. Thin black lines show the phase changes at 410 and 660 km depths. "LVW" is the low-viscosity wedge where the viscosity is lowered. (b) Geometry of the model (B) used to study the position and magnitude of a hot anomaly adjacent to a sinking cold anomaly in internally heated convection (Modified from Morishige *et al.* (2010)). This geometry takes into account the sphericity following van Keken (2001). A depth-dependent viscosity is assumed and we set a low-viscosity at the left and the right corners of the top surface to obtain a plate-like velocity on the top surface. The assumed viscosities are shown by the multiplicity factors of η_{UM} which is the viscosity of the upper mantle. Modified from figures 2 and 5 of *Phys. Earth Planet. Inter.*, *183*, Morishige, M., S. Honda, and M. Yoshida, Possibility of hot anomaly in the sub-slab mantle as an origin of low seismic velocity anomaly under the subducting Pacific plate, 353–365, Copyright 2010, with permission from Elsevier.

analysis, Bagley *et al.* (2009) concluded that the magnitude of the high-temperature anomaly is 155 K. Since the existence of such a hot anomaly adjacent to a cold subducting slab rather contradicts our intuition of a down going flow, it is worth considering its origins.

We have considered two possible causes of the hot anomaly: (A) a hot anomaly, such as a past plume head, came far from the subduction zone (Honda *et al.*, 2007a; Morishige *et al.*, 2010); and (B) a hot anomaly next to a sinking cold anomaly, which is typical in the case of internally heated convection (Morishige *et al.*, 2010).

Figure 17 shows the model settings of both model (A) and model (B). In model (A), we first set the hot anomaly as an initial condition and it is carried by the given velocity of the overlying plate (Fig. 17(a)). The viscosity depends on the temperature. In model (B), the sphericity is considered in 2D annulus models following van Keken (2001) (Fig. 17(b)). The viscosity depends on the depth. To achieve the plate-like movements on the top surface, we assumed a low viscosity region at the top left and top right corners.

Typical cases for both models are shown in Fig. 18(a) (model (A)) and Fig. 18(b) (model (B)) (Morishige *et al.*, 2010).

Originally, Honda *et al.* (2007a) considered that the hot anomaly now observed was the remains of the plume head of a past superplume (Larson, 1991). However, later studies by Morishige *et al.* (2010) showed that the estimate of the residence time of hot anomaly above the 410-km phase boundary in Honda *et al.* (2007a) was too long as a result of neglecting the cooling through the overlying lithosphere. Note that the 410-km phase boundary acts to impede the downward movement of the hot mantle (Honda *et al.*, 2007a), and, thus, it increases the residence time of the hot anomaly, which could be the reason why a good correlation exists between the 410-km seismic discontinuity and the hot anomaly.

Figure 18(a) shows an interesting possibility of the interaction between the slab and the hot anomaly, which has also been shown recently by Liu and Zhou (2015) for the hot asthenosphere model, which is that the asthenosphere everywhere is buoyant, in contrast to our localized hot sub-slab mantle. The slab is hoisted up because of the buoyancy of the hot anomaly. Note that this phenomenon will occur in

doi:10.5047/meep.2017.00502.0035

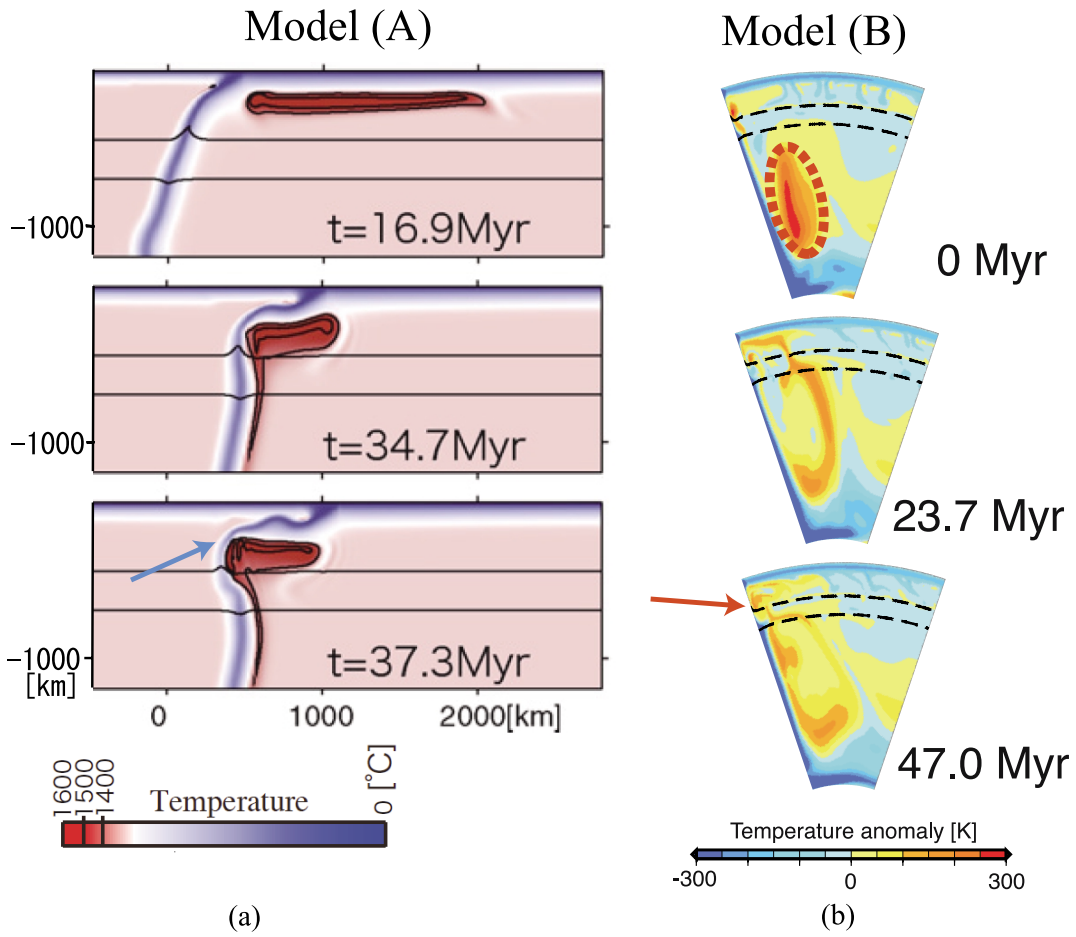

Fig. 18. (a) Results of the temperature field for model (A) (Morishige *et al*., 2010). Note that the slab is hoisted up when the hot anomaly touches the subducting slab (see the arrow). Thin black lines show the phase changes at 410 and 660 km depths. Age shows the time after the start of the run. (b) Results of the distribution of the temperature anomaly, that is, the temperature deviation from the horizontally averaged temperature, for model (B) (Results from Morishige *et al*. (2010)) where the downward flow is occurring along the left wall. Dashed lines show the phase changes at 410 and 660 km depths. Results show only the part near the sinking flow. Note the lower mantle hot anomaly, shown by dotted line and the hot anomaly around the 410 km depth shown by the arrow. Age is the time relative to that of the top figure. Reprinted from figures 3 and 9 of *Phys. Earth Planet. Inter.*, *183*, Morishige, M., S. Honda, and M. Yoshida, Possibility of hot anomaly in the sub-slab mantle as an origin of low seismic velocity anomaly under the subducting Pacific plate, 353–365, Copyright 2010, with permission from Elsevier.

the case of both model (A) and model (B).

The hot temperature anomaly next to the cold downgoing anomaly is typical of internally heated convection. However, the position and the magnitude of such an anomaly depend on the amount of internal heating. Morishige *et al*. (2010) estimated the magnitude and position of the hot anomaly and found that its magnitude could be ∼200 K. Although the hot anomaly is usually located in the lower mantle, it sometimes moves upward and it leaks into the upper mantle (see the sequence shown in Fig. 18(b)). The resultant hot anomaly in the upper mantle is dragged by the overlying lithosphere and it remains for a while in the upper mantle. The timing of occasional upward movements of the hot anomaly is related to the occasional speeding-up of the downward movement of the cold anomaly. From these results, Morishige *et al*. (2010) concluded that the hot anomaly in the sub-slab mantle may have come from the hot anomaly in the lower mantle and is the remains of the leaked hot anomaly in the upper mantle. We will later show that this point is related to the last topic.

6. Nature of the Western Edge of the Stagnant Slab

Tomography models in the western Pacific show the pile of high-speed anomaly around the transition zone (e.g., Fukao *et al*., 1992, 2009). This feature has been commonly interpreted as a result of an interaction between the cold slab and the hindrance nature of the 660-km endothermic phase transition. In early times, the gap between the high-velocity anomaly of the stagnant slab and that in the lower mantle (Fig. 4, Region c) was considered to be the result of the abrupt falling of stagnant slabs (flushing or avalanche), which were shown by 3D numerical simulations (Honda *et al*., 1993; Tackley *et al*., 1993). However, it turned out that the slab morphology depends on the nature of the temperature-dependent viscosity and, especially, the movement of the trench (Christensen, 1996), which may be reflected in the local geologic history. Therefore, we considered the nature of the stagnant slab and the gap (Fig. 4, Regions C and c) by taking into account the geologic history around the Japanese Islands.

doi:10.5047/meep.2017.00502.0035

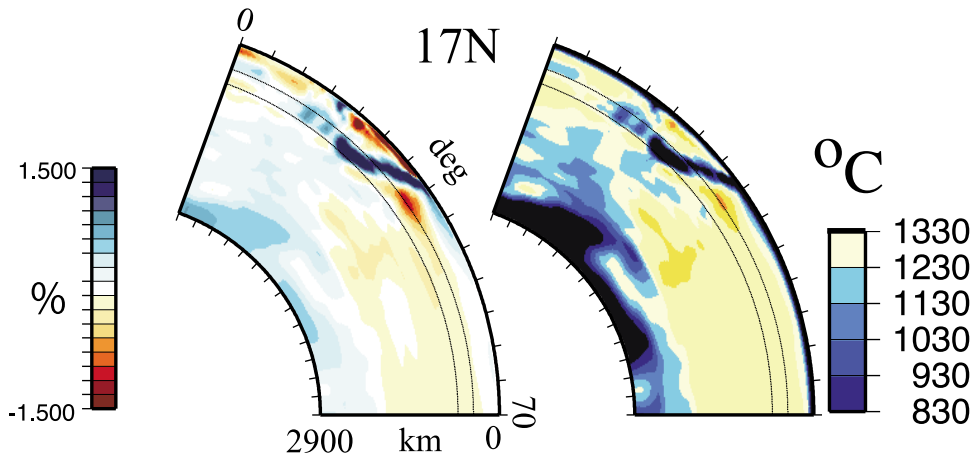

Fig. 19. Comparison between the tomography model (left) and the estimated potential temperature field (right) converted from it using the method described in Honda (2016a).

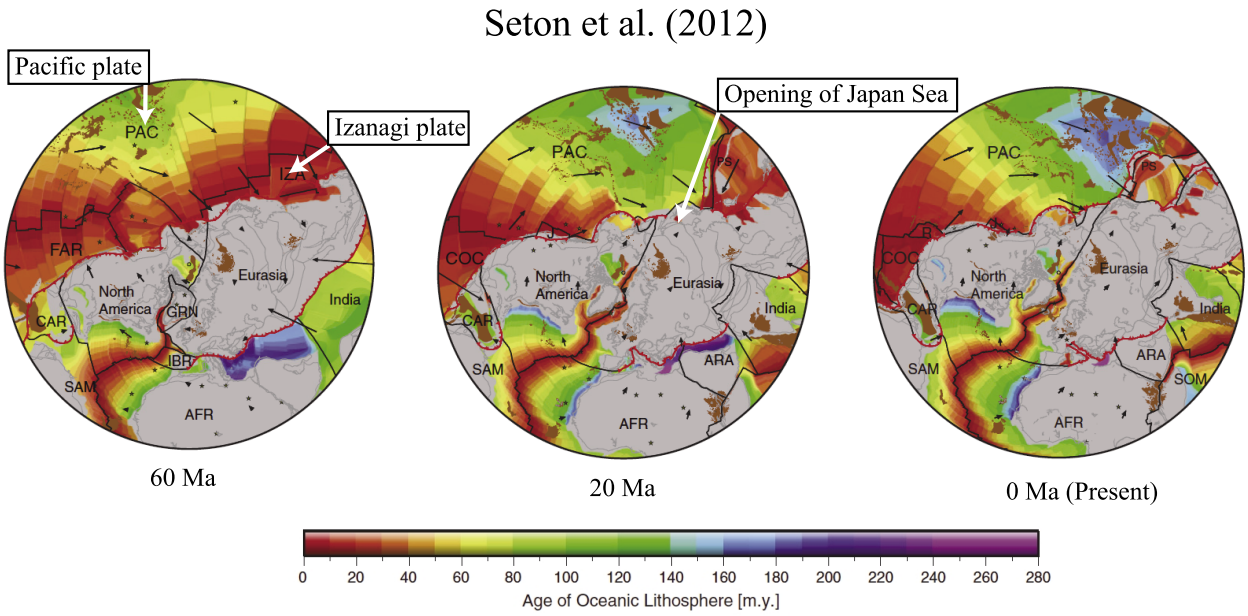

Fig. 20. Reconstruction of plates and the age distribution viewed from the North Pole by Seton *et al.* (2012). Abbreviations are: AFR: African plate, ARA: Arabian plate, CAR: Caribbean plate, COC: Cocos plate, FAR: Farallon plate, GRN: Greenland plate, IBR: Iberian plate, IZA: Izanagi plate, PAC: Pacific plate, PS: Philippine Sea plate, SAM: South America plate, SOM: Somalia plate. Reprinted from figures 25, 27, and 28 of *Earth Sci. Rev.*, *113*, Seton, M., R. D. Muller, S. Zahirovic, C. Gaina, T. Torsvik, G. Shephard, S. Talsma, M. Gurnis, M. Turner, S. Maus, and M. Chandler, Global continental and ocean basin reconstructions since 200 Ma, 212–270, Copyright 2012, with permission from Elsevier.

Honda (2014, 2016a) sought to elucidate these points by applying a simple conversion from the tomography model to the temperature field and using geodynamic modeling with the geologic history taken into account. Honda (2014, 2016a) firstly confirmed the existence of the gap in the potential temperature field converted from the seismic tomography (Fig. 4, Region c, and Fig. 19).

Note that, in the following discussions and in Appendix A, by "temperature" we mean "potential temperature". Figure 19 shows a comparison between the tomography model and the potential temperature field along 17°N. (Note that this is not the actual latitude. It is the latitude when the north pole is set to the pole of the relative motion between the Eurasia plate and the Pacific plate.) The temperature field is estimated by applying the method described in Honda (2016a) to the seismic tomography model NECCES_P1NT (Obayashi *et al.*, 2012). The multiplicity factor of the temperature anomaly, α, estimated from the seismic tomography (see equation (1) of Honda (2016a)), using the conversion coefficient from the seismic velocity anomaly to the temperature anomaly (Karato, 2008), has a different value for a cold anomaly and a hot anomaly, viz. 2.5 (for a cold anomaly) and 1.25 (for a hot anomaly). This means that the slow seismic velocity anomaly, i.e., the high temperature anomaly, is less weighted. α for a cold anomaly is set so that the lowest temperature around the 660 km depth becomes the potential temperature under which earthquakes can occur (Emmerson and McKenzie, 2007). Generally, the converted temperature

doi:10.5047/meep.2017.00502.0035

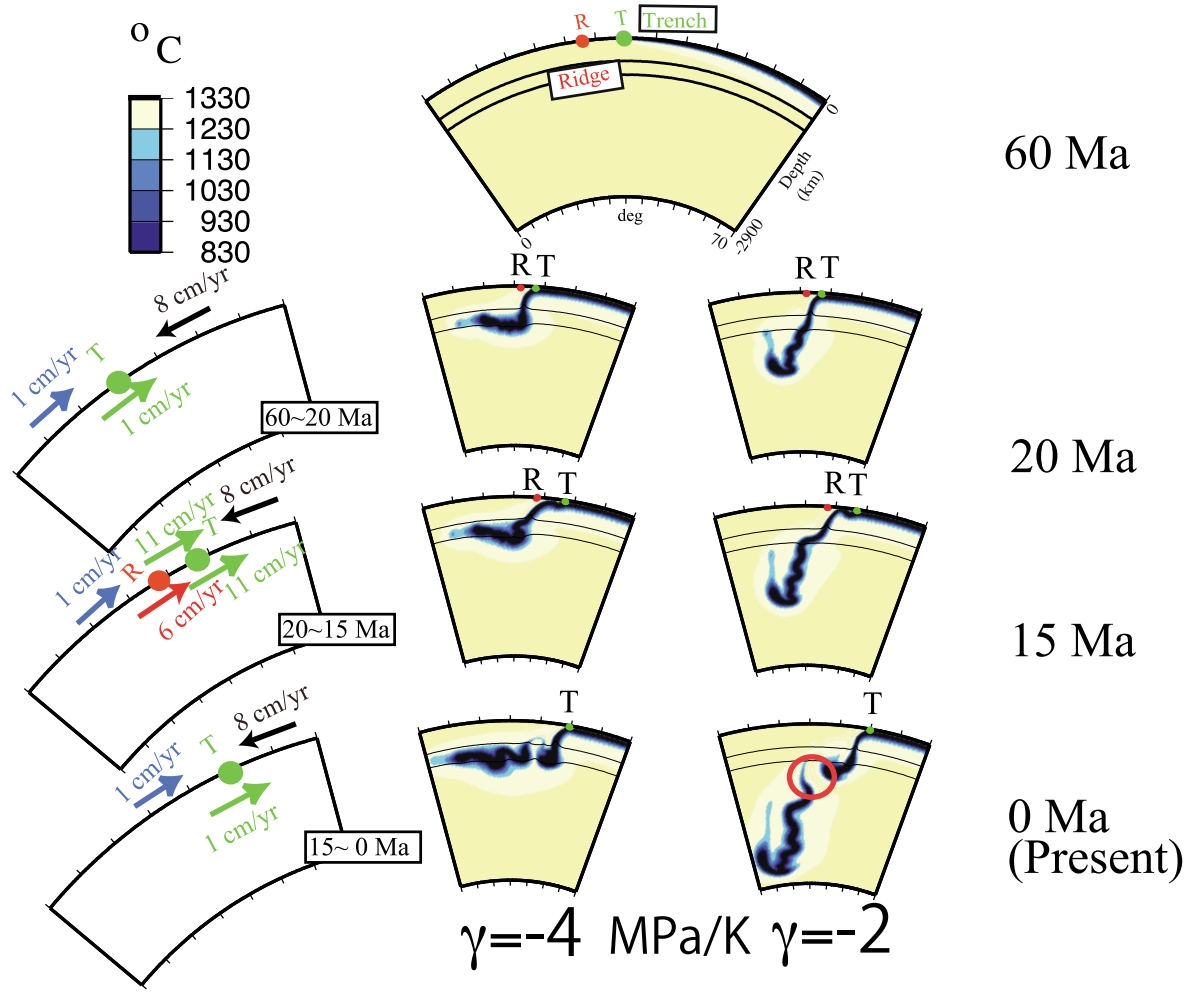

Fig. 21. Results of numerical simulations by Honda (2016a). The left-hand column shows the applied velocity on the top surface of the slab to mimicking the geologic history. Velocities indicated at the upper side of the top surface show the plate velocities and those indicated at the lower side are those of "T" (trench) and "R" (ridge). They define the edges of plates (see the caption of Fig. A1 and Table A1 for details). The initial potential temperature distribution (60 Ma) is given by the top right-hand figure. This is the time when the ridge begins to subduct. Note that we do not model the slab ahead of the ridge. The two lines in the figure show the 410-km and the 660-km phase boundaries. The second and the third columns show the temperature distribution for the cases with a Clapeyron slope of −4 MPa/K and −2 MPa/K at the 660-km phase change, respectively. The red circle indicates a slab gap. We assume that the opening of the Japan Sea began at 20 Ma and stopped at 15 Ma. Reprinted from figure 6 of *Tectonophysics*, *671*, Honda, S., Slab stagnation and detachment under northeast China, 127–138, Copyright 2016, with permission from Elsevier.

field shows slabs which are more continuous than the tomography model does (Honda, 2014).

Major tectonic events of subduction around the Japanese Islands may be summarized as follows (Fig. 20; Seton *et al.* (2012)): (1) Subduction of the ridge which was the plate boundary between the Izanagi plate and the Pacific plate around 50–60 Ma; and (2) opening of the northern part of the Japan Sea which began around 20 Ma and ended around 15 Ma. Using 2D numerical models, Honda (2016a) considered the subduction of the ridge, the subsequent plate movements, the increase of the age of the subducting plate (Sdrolias and Müller, 2006), the opening of the Japan Sea, and the phase changes along the northeast Japan section (Fig. 21). Tectonic movements are mimicked by imposing the velocity on the top surface (see Fig. 21).

Honda (2016a) considered two possibilities of the emergence of the slab gap; (1) a slab gap caused by the subduction of the ridge, and (2) the deformation associated with the opening of the Japan Sea. Comparing the results with observations, it was concluded that (1) is preferable, since (2) predicts a too short present stagnant slab and too small a gap. This conclusion is different from that of Honda (2014), which used quite a simple subduction history and geometry. Another conclusion is that the slope of the Clausius-Clapeyron curve at 660 km is steeper, say −4 MPa/K, than that determined by laboratory experiments of ringwoodite-bridgemanite (plus oxide), say −2 MPa/K or gentler (Katsura *et al.*, 2003). This point was improved in a later model (see below).

Seton *et al.* (2015) also found that the gap was the result of the ridge subduction using 3D models with paleo-reconstruction of the plates and plate movements assimilated, although the model resolution may not be high enough to allow a detailed comparison with tomography models.

doi:10.5047/meep.2017.00502.0035

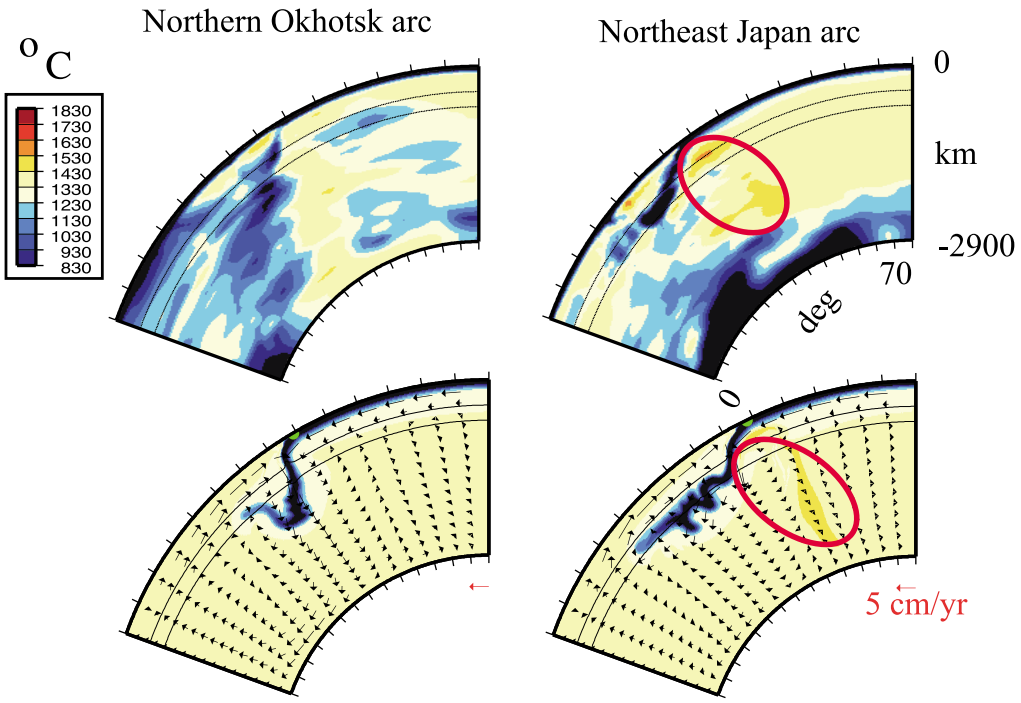

Fig. 22. Comparison between the estimated potential temperature distributions (top row) and the results of numerical simulations (bottom row). The left column and the right column show the northern Okhotsk model and the northeast Japan model, respectively. Results are from Honda (2016b). Note the hot region under the subducting slabs shown by red ovals.

Thus, the western edge of the stagnant slab under northeast China (Fig. 4, Region C) is likely to be a past ridge, or the plate boundary between the Izanagi plate and the Pacific plate, rather than the edge of a broken slab after a flushing or avalanche.

The history of subduction around northeast Japan is similar to that of northern Okhotsk, except for the extent of the back-arc spreading, that is, the subduction of the ridge and the following Pacific plate. However the morphologies of slabs there appear to be quite different, with regard to the significant stagnation under northeast Japan and the fairy continuous slab under northern Okhotsk. These differences may be caused by the difference in convergence velocities, the geometry of the plate boundary as suggested by Morishige and Honda (2013), the extent of the back-arc spreading, and/or the existence of a possible hot anomaly under the northeast Japan arc.

A weakening of the slab may be caused by the grain-size reduction associated with the 410-km phase change (Čížková *et al*., 2002; Tagawa *et al*., 2007; Morishige and Honda, 2013). If the trench retreat is reflected in the back-arc opening, as Honda (2014, 2016a, b) assumed in his modeling, it may not have happened in northern Okhotsk (no or small back-arc opening). On the contrary, it may have happened in northeast Japan (the opening of the Japan Sea). When the ridge subducted, we may expect a change of downgoing flow. Such a change of flow may have triggered the rise of the hot anomaly as shown by Morishige *et al*. (2010).

Honda (2016b) included the effects of the rheological weakening of the slab, the different extent of the back-arc opening and the hot anomaly in the sub-slab mantle, in addition to other effects considered by Honda (2016a) (Fig. 22) with the slope of the Clausius-Clapeyron curve at 660 km being -2 MPa/K.

He concluded that the aforementioned morphological differences are the results of the different degrees of a back-arc opening and the existence/absence of the hot anomaly coupled with the significant rheological weakening of the slab in the transition zone. In his model, the trench retreat and the rheological weakening play a major role in the stagnation of the slab, and the hot anomaly assists the stagnation by shallowing the subduction. Additional results and discussions are given in Appendix A. Future 3D modeling studies, taking into account the different subduction angle as observed by Morishige and Honda (2013) and the detailed geologic history, will be fruitful for understanding the geological and geophysical implications of the seismic tomography around the Japanese Islands.

7. Final Remarks

Generally speaking, two extreme approaches exist in Earth Sciences. One is based on the descriptions of observations, and the other is based on the appreciations of fundamental physics and/or chemistry. The characteristics of these two approaches are quite different. For example, the latter approach tends to seek clarification of the general principles of geologic phenomena, while the former does not necessarily do so. The understanding of Earth Sciences is located between these two extreme approaches and numerical simulations are appropriate tools to link both approaches. Thus, we believe that the developments of numerical models will contribute to the general advancement of the Earth Sciences.

doi:10.5047/meep.2017.00502.0035

Regarding the development of models, the increase of observations and the improving quality of data change the models. Early models were rather conceptual and general. As available data, such as heat flow, increased, models were modified to explain those observations. 3D information such as seismic tomography and seismic anisotropy introduced the 3D modeling of subduction zones and the geologic history led to the modeling of temporally and spatially changing subduction zones. One important topic, which we do not discuss extensively in this review, is the chemical aspects and those related to the subduction processes such as the movement of fluid, that of melt and the melting processes (a brief discussion is given in Appendix B). This is mainly because we try to understand the limits of the application of simple models. The other reason is that it appears that we still do not have a "standard model" of such processes considering a variety of studies. This will be clarified by future theoretical works strongly coupled to observational studies. The models presented in this review may change in the future, as has been the case with previous models. It is, however, pleasing that the models presented here serve as a basis for a further understanding of the subduction zones.

Acknowledgments. I thank Takeyoshi Yoshida and Manabu Morishige who contributed to many parts of this review. Manabu Morishige helped me to draw new figures from previous works. Masayuki Obayashi provided me with NECCESS_P1NT model and Akiko Tanaka sent me the new heat flow data. Paul Tackley and Masaki Yoshida supported the mainly technical aspects of numerical simulations. I enjoyed discussions (and drinking) with Dave Yuen very much. I appreciated the encouragement of Tetsuzo Seno and Hitoshi Kawakatsu. Suggestive comments were provided by Hikaru Iwamori and an anonymous reviewer. Especially, Appendix B owes much to the comments of Hikaru Iwamori, although the content is totally my responsibility. Finally, I thank Prof. Hiroo Kanamori and Michio Tagawa for their editorial works and managements. The Generic Mapping Tools (Wessel and Smith, 1998) were used to construct many of the figures. Computations were carried out at Earthquake Information Center, Earthquake Research Institute, The University of Tokyo.

Appendix A.

We describe more details of the results presented in Honda (2016b). The model is essentially the same one as described in Honda (2016a). Honda (2016b) considered the models of "Northern Okhotsk" and "Northeast Japan". The history of subduction of each region is mimicked by applying the plate velocity on the top surface (Fig. A1) and is tabulated in Table A1.

The law of viscosity is that as described in Honda (2016a) with the addition of the rheological weakening of the slab in the transition zone, and is given by

$$\eta = \begin{cases} \eta\,(T, z, \sigma_Y)\, r^{\left(\frac{T-T_{\max}}{T_{\max}-T_{\min}}\right)^p} & (T_{\min} < T < T_{\max}) \\ \eta\,(T, z, \sigma_Y) & (\text{otherwise}) \end{cases} \tag{A.1}$$

where η is the effective viscosity, $\eta\,(T, z, \sigma_Y)$ is the viscosity of type (A) with an activation energy of 120 kJ/mol as described in Honda (2016a), T is the temperature, z is the depth, σ_Y is the yield stress, $r = 0.01$ and $p = 2.5$ are constants and $T_{\max} = 850°\text{C}$ and $T_{\min} = 600°\text{C}$. The multiplier of $\eta\,(T, z, \sigma_Y)$ is based on the rheological weakening by the grain-size reduction through the phase change (e.g., Čížková *et al.*, 2002; Tagawa *et al.*, 2007; Morishige and Honda, 2013). However, it should be regarded as a parameterization of the rheological weakening of the slab rather than an application of experimental results. The depth of the plate boundary (d_p in Honda (2016a)) is set to be 100 km and σ_Y below a 100 km depth is 500 MPa, which is equivalent to the effective friction coefficient of ∼0.1 above 100 km depth. This σ_Y is higher than that used before (100∼200 MPa: Honda, 2014, 2016a) to avoid the break-up of the subducting slab by the hot anomaly (see the arrow in Fig. 18). As a result, the rheological weakening of the slab is required for the slab to stagnate in the transition zone, as shown in Fig. A2.

Table A1. Surface speed of plates

Northern Okhotsk model				
Time (Ma)	50	20	15	0 (Present)
V_{op}: speed[1] of "overlying plate" (cm/yr)	1	1	1	1
V_{sub}: speed[1] of "subducting plate" (cm/yr)	6	6	6	6
Age of "subducting plate"[2] (Myr)	0	40	30	100
Northeast Japan model				
Time (Ma)	50	20	15	0 (Present)
V_{op}: speed[1] of "overlying plate" (cm/yr)	1	1	1	1
V_{tr}: speed[1] of "trench" (cm/yr)	1	11	11	1
V_{rg}: speed[1] of "ridge" (cm/yr)	—	6	6	—
V_{sub}: speed[1] of "subducting plate" (cm/yr)	8	8	8	8
V_{sr}: spreading rate (cm/yr)	0	10	10	0
Age of "subducting plate"[2] (Myr)	0	48	36	120

[1]Positive toward the trench. Speeds of "T" (V_{rg}) and "R" (V_{tr}) are given by:

$$V_{rg} = V_{sr}/2 + V_{op}$$
$$V_{tr} = \begin{cases} V_{op} & (\text{Without spreading}) \\ V_{op} + V_{sr} & (\text{With spreading}) \end{cases}$$

See Honda (2016a) for details.
[2]Age at the trench. It increases linearly from the time of the ridge subduction to the present.

Figure A2 shows the results of the northern Okhotsk model without (Fig. A2(a)) and with (Fig. A2(b)), rheological weakening of the slab. The times 50, 20, 15 and 0 Ma correspond, respectively, to the time when the ridge started to subduct, the time when the opening of the Japan Sea began, the time when the opening of the Japan Sea stopped, and the present. These figures show the continuous slab from the upper to the lower mantle both with and without the rheological weakening of the slab. Note that we do not take into account the slab ahead of the ridge, i.e., the Izanagi plate. This is mainly because we do not know much about the nature of the Izanagi plate. It should be noted that it may affect the results, even though the ridge separated the Izanagi plate from the Pacific plate. This should be studied in the future.

Figure A3 shows the results of the northeast Japan model without (Fig. A3(a)), and with (Fig. A3(b)) rheological weakening of the slab. The main difference between this model and the northern Okhotsk model is the existence of the

doi:10.5047/meep.2017.00502.0035

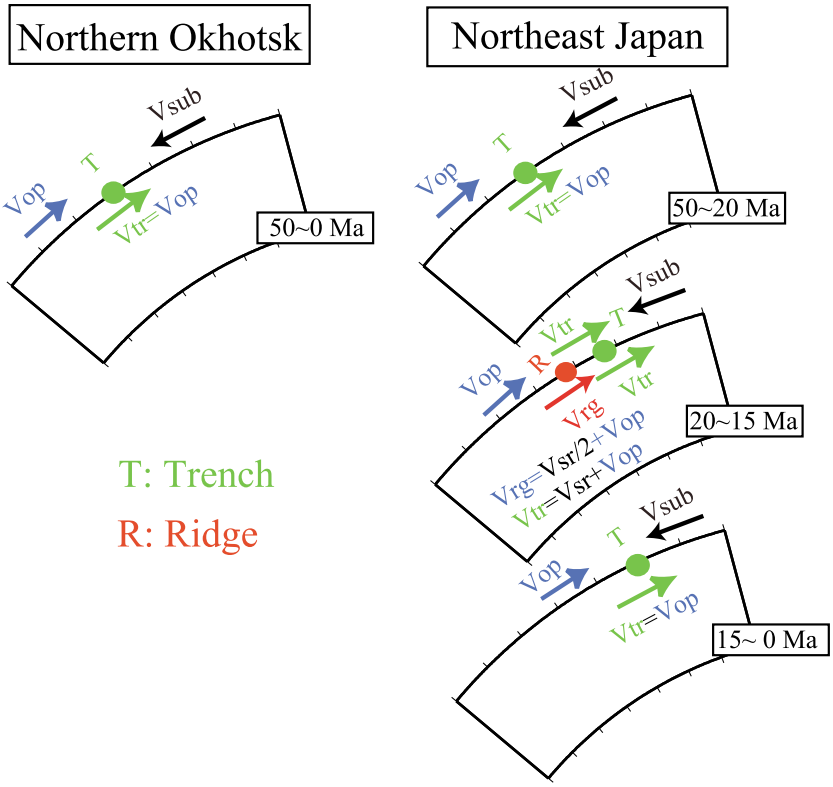

Fig. A1. Velocity boundary conditions on the top surface for the northern Okhotsk case (left column) and the northeast Japan case (right column). "T" is "trench" which is the right edge of the "overlying plate" or "back-arc plate". To the right of "T" is the "subducting plate". "R" is "ridge" which is the spreading center of the opening of the Japan Sea. The section between "R" and "T" is the "back-arc plate". V_{op} and V_{sub} are the speeds of the "overlying plate" and the "subducting plate", respectively. V_{tr}, V_{rg} and V_{sr} are the speeds of "T", "R" and the spreading rate of the back-arc basin, i.e., the Japan Sea. Further details are given in Table A1.

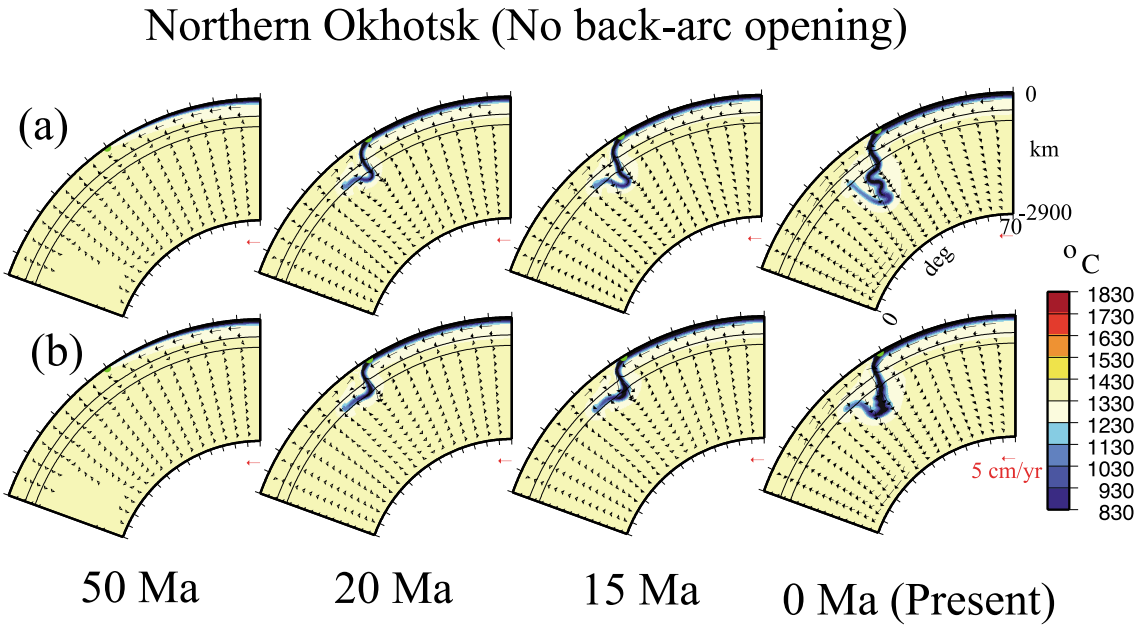

Fig. A2. Results of the potential temperature field for the northern Okhotsk model. Arrows show the velocity and the thin lines show the 410-km and the 660-km phase boundaries. The upper and the lower rows show the cases without, and with, rheological weakening of the slab in the transition zone, respectively. The initial state (50 Ma) assumes the start of the subduction of the ridge. Results are from Honda (2016b).

doi:10.5047/meep.2017.00502.0035

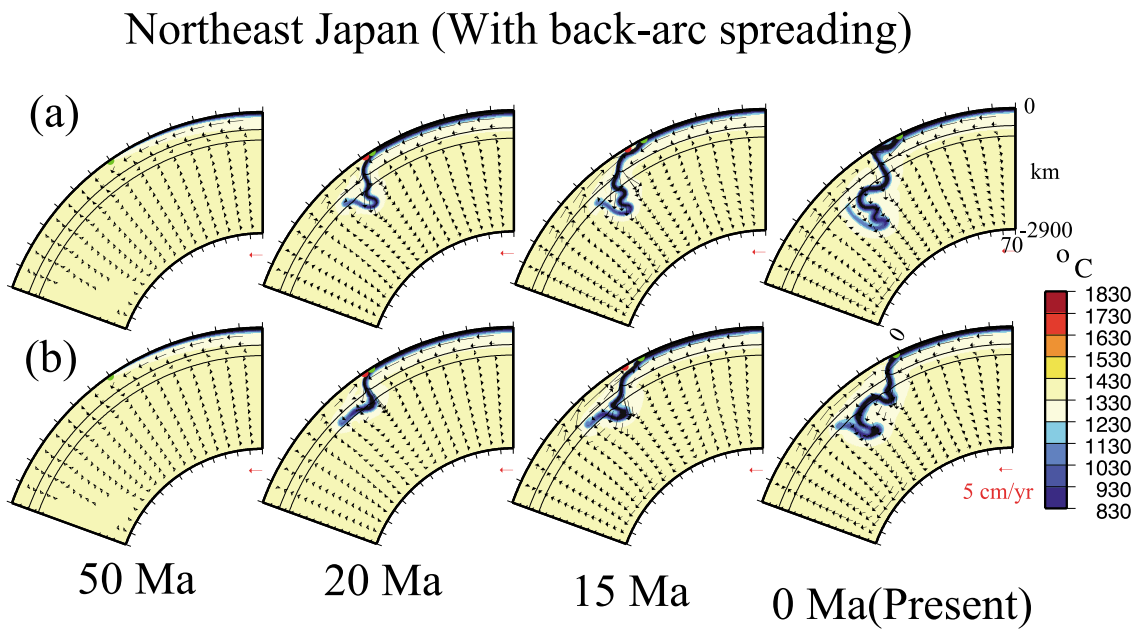

Fig. A3. Results of the potential temperature field for the northeast Japan model. Arrows show the velocity and the thin lines show the 410-km and the 660-km phase boundaries. The upper and lower rows show the cases without, and with, rheological weakening of the slab in the transition zone. The initial state (50 Ma) assumes the start of the subduction of the ridge. The opening of the Japan Sea is assumed to have occurred between 15 Ma and 10 Ma. Results are from Honda (2016b).

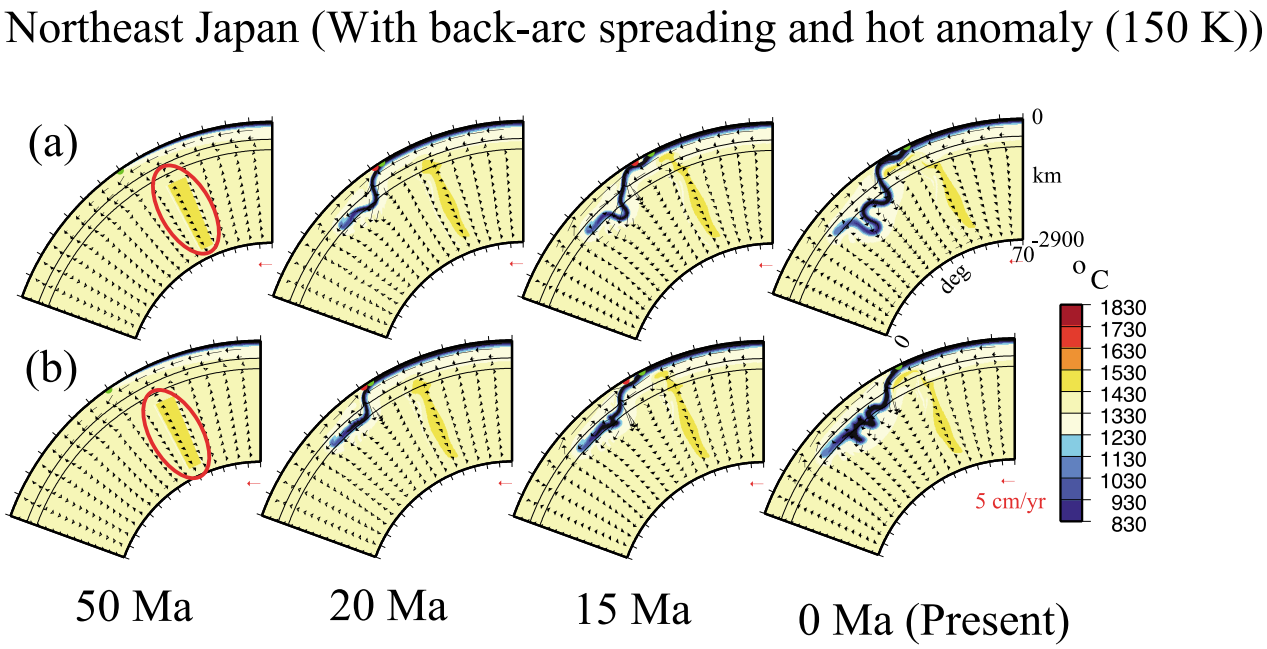

Fig. A4. Results of the northeast Japan model with a hot anomaly (see red circles). Arrows show the velocity and the thin lines show the 410-km and the 660-km phase boundaries. The upper and lower rows show the cases without, and with, rheological weakening of the slab in the transition zone, respectively. The initial state (50 Ma) assumes the start of the subduction of the ridge. The opening of the Japan Sea is assumed to have occurred between 15 Ma and 10 Ma. Results are from Honda (2016b).

back-arc opening from 20 to 15 Ma for the northeast Japan model. The trench retreat tends to make the slab stagnant in the transition zone and the addition of the rheological weakening of the slab enhances this tendency more.

Figure A4 shows the same case as that shown in Fig. A3 with the hot anomaly in the sub-slab mantle, which is set as an initial condition (see the red circles in Fig. A3). The magnitude of the hot anomaly is set to be 150 K and its initial distribution is shown in the "50 Ma" column of Fig. A4. Comparing this with the case without hot anomaly, the hot anomaly further enhances the stagnation of the slab in the upper mantle. Note that the magnitude and the initial position of the hot anomaly are essentially unknown. We only know the present location and the possible magnitude of the

doi:10.5047/meep.2017.00502.0035

hot anomaly. Hence, we attempted to set their position and geometry simple enough by taking into account the results of Morishige *et al*. (2010) under the limitation that the final results are reasonably similar to the present status.

Appendix B.

Model studies treating the fluid and the melting processes in the mantle wedge are quite important, since they have the potential to explain the origin and distribution of volcanoes—the first-order observations of geologic phenomena. A variety of the models are presented and discussed currently because of the complexity of problems. Roughly speaking, there are three major issues relating to this topic: (1) the amount of fluid based on the determination of the phase diagram; (2) the rheological behavior of fluid and fluid-bearing rocks; and (3) the transportation mechanism of the fluid. Probably, the first point is most accurately determined based on the experimental and theoretical approach (e.g., Iwamori, 1998) assuming that the composition of the material is appropriately inferred, but there still exists problems such as to what extent the slab was chemically affected by the sea-water–rock interaction. The second point may be determined experimentally (e.g., Karato and Jung (2003)), but not as accurately as the determination of phase diagrams. The third point is probably the most uncertain, since it is quite difficult to verify it based on both experiments/observations and theories. Currently, the most popular model appears to be the porous flow model (e.g., McKenzie, 1984) which may be appropriate given that the amount of fluid/melt is small. While Spiegelman and McKenzie (1987) showed that the pressure gradient in the deforming mantle plays an important role, many models assume that the pressure difference in Darcy's law only comes from the density difference between fluid and the solid. It is not our intention to review the above three topics in detail. Rather, we pay attention to the fluid and viscosity distribution of the models taking into account the fluid explicitly.

As far as we know, the model which may show or suggest the finger-like distribution of volcanoes (gravitational instability of the boundary layer), is a 2D model developed by Arcay *et al*. (2005). Several conceptual models have been proposed recently by Wada *et al*. (2015). The general pattern of the fluid distribution is its almost ubiquitous existence in the corner of the mantle wedge and the comparatively thin tail above the subducting slab (Arcay *et al*., 2005; Cagnioncle *et al*., 2007; Hebert *et al*., 2009; Wilson *et al*., 2014; Horiuchi and Iwamori, 2016). However, the detail is different, which may come from the assumed transportation mechanism and the composition and temperature structure of the subducting slab. Wilson *et al*. (2014) showed that the inclusion of the pressure term, which is neglected in many studies, can modify the fluid distribution and may lead to a focusing of the fluid. Horiuchi and Iwamori (2016) applied their model to the arc volcanism of northeast Japan. The fluid distribution of their preferred model is similar to the geometry of our LVW. Note that we usually do not consider the tail above the subducting slab, except in a case which is briefly mentioned in Honda (2011) where it was shown that such a tail may explain the migration speed of the volcano distribution from the back-arc to the trench more naturally.

Although the geometry of the LVW is similar to the fluid distribution derived from a more-or-less self-consistent model of fluid distribution, the obtained viscosity is higher (usually by an order of magnitude) than that which is necessary to explain the hot fingers ($O(10^{18}$ Pa·s). From an observational basis, viscoelastic modeling of time-dependent deformation near the subduction zone shows that the viscosity of the uppermost mantle is around 10^{19} Pa·s (Wang, 2007). For northeast Japan, it is estimated to be between 0.4 to 1.3 $\times$ 10^{19} Pa·s which is marginal to our model of LVW. A model of Arcay *et al*. (2005) shows $O(10^{18})$ Pa·s in the fluid-filled region (their Fig. 12(c)). Models of Hebert *et al*. (2009) and Horiuchi and Iwamori (2016) show a generally higher viscosity in the uppermost mantle wedge ($\sim 10^{20}$ Pa·s). Thus, at present, the models are not entirely consistent with present observations and/or analyses.

There are a several missing considerations in these modeling studies. They do not consider the temporal change in the environment surrounding the subduction zone. For example, in northeast Japan, the active back-arc opening occurred around $\sim$20 Ma (Yoshida *et al*., 2013). This situation was taken into account in our SSC model by changing the temperature boundary condition of the back-arc side. The change of slab dip may also affect the results (Honda *et al*., 2007b). Thus, it may be erroneous to treat a variety of geologic phenomena as a general feature of subduction zone, and careful evaluation and analyses of observations are necessary.

References

Andrews, D. J., and N. H. Sleep (1974), Numerical modelling of tectonic flow behind island arcs, *Geophys. J. R. Astron. Soc.*, *38*, 237–251.

Arcay, D., E. Tric, and M.-P. Doin (2005), Numerical simulations of subduction zones Effects of slab dehydration on the mantle wedge dynamics, *Phys. Earth Planet. Inter.*, *149*, 133–153.

Bagley, B., A. M. Couryier, and J. Revenaugh (2009), Melting in the deep upper mantle oceanward of the Honshu Slab. *Phys. Earth Planet. Inter.*, *25*, 3231–3234.

Batchelor, G. K. (1967), *An Introduction to Fluid Dynamics*, Cambridge Univ. Press, pp. 615.

Cagnioncle, A.-M., E. M. Parmentier, and L. T. Elkins-Tanton (2007), Effect of solid flow above a subducting slab on water distribution and melting at convergent plate boundaries, *J. Geophys. Res.*, *112*, B09402, doi:10.1029/2007JB004934.

Christensen, U. (1996), The influence of trench migration on slab penetration into the lower mantle, *Earth Planet. Sci. Lett.*, *140*, 27–39.

Čížková, H., J. van Hunen, and A. P. van den Berg (2002), The influence of rheological weakening and yield stress on the interaction of slabs with the 670 km discontinuity, *Earth Planet. Sci. Lett.*, *199*, 447–457.

DeMets, C., R. G. Gordon, D. F. Argus, and S. Stein (1994), Current plate motions, *Geophys. J. Int.*, *101*, 425–478.

Emmerson, B., and D. P. McKenzie (2007), Thermal structure and seismicity of subducting lithosphere, *Earth Planet. Sci. Lett.*, *163*, 191–208.

Fukao, Y., M. Obayashi, H. Inoue, and M. Nenbai (1992), Subducting slabs stagnant in mantle transition zone, *J. Geophys. Res.*, *97*, 4809–4822.

Fukao, Y., M. Obayashi, T. Nakakuki, and the Deep Slab Project Group (2009), Stagnant slab: A review, *Ann. Rev. Earth Planet. Sci.*, *37*, 19–46.

Gerya, T. V., and D. A. Yuen (2003), Rayleigh-Taylor instabilities from hydration and melting propel 'cold plumes' at subduction zones, *Earth Planet. Sci. Lett.*, *212*, 47–62.

Hasebe, K., N. Fujii, and S. Uyeda (1970), Thermal processes under island arcs, *Tectonophysics*, *10*, 335–355.

Hasegawa, A., and J. Nakajima, J. (2004), Geophysical constraints on slab

doi:10.5047/meep.2017.00502.0035

subduction and arc magmatism, in *The State of the Planet: Frontiers and Challenges in Geophysics*, Geophysical Monograph 150, IUGG Vol. 19, pp 81–93.

Hashimoto, C., K. Fukui, and M. Matsu'ura (2004), 3-D modeling of plate interfaces and numerical simulation of long-term crustal deformation in and around Japan, *Pure Appl. Geophys.*, *161*, 2053–2067.

Hebert, L. B., P. Antoshechkina, P. Asimow, and M. Gurnis (2009), Emergence of a low-viscosity channel in subduction zones through the coupling of mantle flow and thermodynamics, *Earth Planet. Sci. Lett.*, *278*, 243–256.

Honda, S. (1985), Thermal structure beneath Tohoku, northeast Japan—A case study for understanding the detailed thermal structure of the subduction zone, *Tectonophysics*, *112*, 69–102.

Honda, S. (2008), A simple semi-dynamical model of the subduction zones: effects of a moving plate boundary on the small-scale convection under the island arc, *Geophys. J. Int.*, *173*, 1095–1105.

Honda, S. (2009), Numerical simulations of mantle flow around slab edges, *Earth Planet. Sci. Lett.*, *277*, 112–122.

Honda, S. (2011), Planform of small-scale convection under the island arc, *Geochem. Geophys. Geosyst.*, *12*, Q11005, doi:10.1029/2011GC003827.

Honda, S. (2014), Strength of slab inferred from the seismic tomography and geologic history around the Japanese Islands, *Geochem. Geophys. Geosyst.*, *15*, 1333–1347, doi:10.1002/2014GC005225.

Honda, S. (2016a), Slab stagnation and detachment under northeast China, *Tectonophysics*, *671*, 127–138.

Honda, S. (2016b), Morphology of the stagnant slab from the northern Okhotsk arc to the northeastern Japan arc and its geodynamic implications, Abstract SIT11-P08 presented at the Japan Geoscience Union Meeting Meeting 2016, Makuhari, Chiba, Japan, 24 May.

Honda, S., and M. Saito (2003), Small-scale convection under the back-arc occurring in the low viscosity wedge, *Earth Planet. Sci. Lett.*, *216*, 703–715.

Honda, S., and T. Yoshida (2005a), Application of the model of small-scale convection under the island arc to the NE Honshu subduction zone, *Geochem. Geophys. Geosyst.*, *6*, Q01002, doi:10.1029/2004GC000785.

Honda, S., and T. Yoshida (2005b), Effects of oblique subduction on the 3-D pattern of small-scale convection within the mantle wedge, *Geophys. Res. Lett.*, *32*, L13307, doi:10.1029/2005GL0023106.

Honda, S., D. A. Yuen, S. Balachandar, and D. Reuteler (1993), Three dimensional instabilities of mantle convection with multiple phase transitions, *Science*, *259*, 1308–1311.

Honda, S., M. Saito, and T. Nakakuki (2002), Possible existence of small-scale convection under the back-arc, *Geophys. Res. Lett.*, *29*, 2043, doi:10.1029/2002GL015853.

Honda, S., M. Morishige, and Y. Orihashi (2007a), Sinking hot anomaly trapped at the 410 km discontinuity near the Honshu subduction zone, Japan, *Earth Planet. Sci. Lett.*, *261*, 565–577.

Honda, S., T. Yoshida, and K. Aoike (2007b), Spatial and temporal evolution of arc volcanism in the northeast and Izu-Bonin arcs: Evidence of small-scale convection under the island arc?, *Island Arc*, *16*, 214–223.

Honda, S., T. Gerya, and G. Zhu (2010), A simple three-dimensional model of thermo-chemical convection in the mantle wedge, *Earth Planet. Sci. Lett.*, *290*, 311–318.

Horiuchi, S., and H. Iwamori (2016), A consistent model for fluid distribution, viscosity distribution, and flow-thermal structure in subduction zone, *J. Geophys. Res. Solid Earth*, *121*, 3238–3260, doi:10.1002/2015JB012384.

Iwamori, H. (1998), Transortation of H_2O and melting in subduction zones, *Earth Planet. Sci. Lett.*, *160*, 65–80.

Jung, H., and S. Karato (2001), Water-induced fabric transition in olivine, *Science*, *293*, 1460–1463.

Karato, S. (2008), *Deformation of Earth Materials*, Cambridge Univ. Press, pp 463.

Karato, S., and H. Jung (2003), Effects of pressure on high-temperature dislocation creep in olivine, *Philos. Mag.*, *83*, 401–414.

Karato, S., and P. Wu (1993), Rheology of the upper mantle: a synthesis, *Science*, *260*, 771–778.

Katsura, T., H. Yamada, T. Shinmei, A. Kubo, S. Ono, M. Kanzaki, A. Yoneda, M. J. Walter, E. Ito, S. Urakawa, K. Funakoshi, and W. Utsumi (2003), Post-spinel transition in $Mg{-}2SiO_4$ determined by high P-T in situ X-ray diffractiometry, *Phys. Earth Planet. Inter.*, *136*, 11–24.

Kneller, E. A., and P. E. van Keken (2008), Effects of three-dimensional slab geometry on deformation in the mantle wedge: implications for shear wave anisotropy, *Geochem. Geophys. Geosyst.*, *9*, Q01003, doi:10.1029/2007GC001677.

Kneller, E. A., P. E. van Keken, S. Karato, and J. Park (2005), B-type olivine fabric in the mantle wedge: insights from high-resolution non-Newtonian subduction zone models, *Earth Planet. Sci. Lett.*, *237*, 781–797.

Kondo, H., K. Kaneoka, and K. Tanaka (1998), Characterization of spatial and temporal distribution of volcanoes since 14 Ma in the Northeast Japan arc, *Bull. Volcanol. Soc. Jpn.*, *43*, 173–180.

Long, M. D., and P. G. Silver (2008), The subduction zone flow field from seismic anisotropy: A global view, *Science*, *319*, 315–318.

Larson, R. L. (1991), Latest pulse of Earth: Evidence for a mid-Cretaceous superplume. *Geology 19*, 547–550.

Liu, L., and Q. Zhou (2015), Deep recycling of oceanic asthenosphere material during subduction, *Geophys. Res. Lett.*, *42*, 2204–2211, doi:10.1003/2015GL063633.

McKenzie, D. P. (1967), Some remarks on heat flow and gravity anomalies, *J. Geophys. Res.*, *72*, 6261–6273.

McKenzie, D. P. (1969), Speculations on the consequences and causes of plate motions, *Geophys. J. R. Astron. Soc.*, *18*, 1–32.

McKenzie, D. P. (1984), The generation and compaction of partially molten rock, *J. Petrol.*, *25*, 713–763.

Minear, J. W., and M. N. Toksöz (1970), Thermal regime of a downgoing slab and new global tectonics, *J. Geol. Res.*, *75*, 1397–1419.

Morishige, M. (2015), A new regime of slab-mantle coupling at the plate interface and its possible implications for the distribution of volcanoes, *Earth Planet. Sci. Lett.*, *427*, 262–271.

Morishige, M., and S. Honda (2011), Three-dimensional structure of P-wave anisotropy in the presence of small-scale convection in the mantle wedge, *Geochem. Geophys. Geosyst.*, *12*, Q12010, doi:10.1029/2011GC003866.

Morishige, M., and S. Honda (2013), Mantle flow and deformation of subducting slab at a plate junction, *Earth Planet. Sci. Lett.*, *365*, 132–142.

Morishige, M., S. Honda, and M. Yoshida (2010), Possibility of hot anomaly in the sub-slab mantle as an origin of low seismic velocity anomaly under the subducting Pacific plate, *Phys. Earth Planet. Inter.*, *183*, 353–365.

Nakajima, J., J. Shimizu, S. Hori, and A. Hasegawa (2006), Shear-wave splitting beneath the southwestern Kurile arc and northeastern Japan arc: A new insight into mantle return flow, *Geophys. Res. Lett.*, *33*, L05305, doi:10.1029/2005GL025053.

Obayashi, M., H. Sugioka, J. Yoshimitsu, and Y. Fukao (2006), High temperature anomalies oceanward of subducting slabs at the 410-km discontinuity, *Earth Planet. Lett.*, *243*, 149–158.

Obayashi, M., H. Kawakatsu, S. Tanaka, Y. J. Chen, J. Ning, S. P. Grand, F. Niu, K. Miyakawa, K. Idehara, T. Tonegawa, R. Iritan (2012), P-wave tomography of Northeastern China observed with NECESSArray. Abstract S24B-06 presented at 2011 Fall Meeting, AGU, San Francisco, Calif., 5–9 Dec.

Peyton, V., V. Levin, J. Park, M. Brandon, J. Lees, E. Gordeev, and A. Ozerov (2001), Mantle flow at a slab edge: Seismic anisotropy in the Kamchatka region, *Geophys. Res. Sci. Lett.*, *28*, 379–382.

Richter, F. M., and B. Parsons (1975), On the interaction of two scales of convection in the mantle, *J. Geophys. Res.*, *80*, 2529–2541.

Sdrolias, M., and M. Müller (2006), Controls on back-arc basin formation, *Geochem. Geophys. Geosyst.*, *7*, Q04016, doi:10.1029/2005GC001090.

Seno, T., and T. Sakurai (1996), Can the Okhotsk plate be discriminated from the North America plate?, *J. Geophys. Res.*, *101*, 11305–11315.

Seno, T., S. Stein, and A. E. Gripp (1993), A model for the motion of the Philippine Sea plate consistent with NUVEL-1 and geological data, *J. Geophys. Res.*, *98*, 17941–17948.

Seton, M., R. D. Muller, S. Zahirovic, C. Gaina, T. Torsvik, G. Shephard, S. Talsma, M. Gurnis, M. Turner, S. Maus, and M. Chandler (2012), Global continental and ocean basin reconstructions since 200 Ma, *Earth Sci. Rev.*, *113*, 212–270.

Seton, M., N. Flament, J. Whittaker, R. D. Muller, M. Gurnis, and D. J. Bower (2015), Ridge subduction sparked reorganization of the Pacific plate-mantle system 60-50 million years ago, *Geophys. Res. Lett.*, *42*, 1732–1740, doi:10.1002/2015GL063057.

Spiegelman, M., and D. McKenzie (1987), Simple 2-D model for melt extraction at mid-ocean ridges and island arcs, *Earth Planet. Sci. Lett.*, *83*, 137–152.

Stevenson, D. J., and J. S. Turner (1977), Angle of subduction, *Nature*, *270*, 334–336.

Tackley, P. J. (2000), Self-consistent generation of tectonic plates in

doi:10.5047/meep.2017.00502.0035

time-dependent, three-dimensional mantle 1. Pseudoplastic yielding, *Geochem. Geophys. Geosyst.*, *1*, Paper number 2000GC000036.
Tackley, P. J., D. J. Stevenson, G. A. Glatzmaier, and G. Schubert (1993), Effects of an endothermic phase transition at 670 km depth in a spherical model of convection in the Earth's mantle, *Nature*, *361*, 699–704.
Tagawa, M., T. Nakakuki, and F. Tajima (2007), Dynamical modeling of trench retreat driven by the slab interaction with the mantle transition zone, *Earth Planets Space*, *59*, 65–71.
Tamura, Y., Y. Tatsumi, D. Zhao, Y. Kido, and H. Shukuno (2002), Hot fingers in the mantle wedge: new insights into magma genesis in subduction zones, *Earth Planet. Sci. Lett.*, *197*, 105–116.
Tanaka, A., M. Yamano, Y. Yano, and M. Sasada (2004), Geothermal Gradient and Heat Flow Data in and around Japan, *Digital Geoscience Map*, *DGM P-5*, Geological Survey of Japan.
Toksöz, M. N., J. W. Minear, and B. R. Julian (1971), Temperature field and geophysical effects of downgoing slab, *J. Geophys. Res.*, *76*, 1113–1138.
Torii, Y., and S. Yoshioka (2007), Physical conditions producing slab stagnation: Constraints of the Clapeyron slope, mantle viscosity, trench retreat, and dip angles, *Tectonophysics*, *445*, 200–209.
van der Hilst, R., and T. Seno (1993), Effects of relative plate motion on the deep structure and penetration depth of slabs below the Izu-Bonin and Mariana island arcs, *Earth Planet. Sci. Lett.*, *120*, 395–407.
van Hunen, J., and O. Čadek (2009), Reduced oceanic seismic anisotropy by small-scale convection, *Earth Planet. Sci. Lett.*, *284*, 622–629.
van Keken, P. E. (2001), Cylindrical scaling for dynamical cooling models of the Earth, *Phys. Earth Planet. Inter.*, *124*, 119–130.
Wada, I., J. He, A. Hasegawa, and J. Nakajima (2015), Mantle wedge flow pattern and thermal structure in Northeast Japan: Effects of oblique subduction and 3-D slab geometry, *Earth Planet. Sci. Lett.*, *426*, 76–88.
Wang, K. (2007), Elastic and viscoelastic model of subduction earthquake cycles, in *The Seismogenic Zone of Subduction Thrust Faults*, edited by T. H. Dixon and J. C. Moore, Columbia Univ. Press, New York, pp. 540–575.
Wessel, P., and W. H. F. Smith (1998), New improved version of the Generic Mapping Tools released, *Eos Trans. AGU*, *79* (47), 579.
Wilson, C. R., M. Spiegelman, P. E. van-Keken, and B. R. Hacker (2014), Fluid flow in subduction zones: The role of solid rheology and compaction pressure, *Earth Planet. Sci. Lett.*, *401*, 261–274.
Yoshida, T., J.-I. Kimura, R. Yamada, V. Acocella, H. Sato, D. Zhao, J. Nakajima, A. Hasegawa, T. Okada, S. Honda, M. Ishikawa, O. D. A. Prima, T. Kudo, B. Shibazaki, A. Tanaka, and T. Imaizumi (2013), Evolution of late Cenozoic magmatism and crust-mantle structure in the NE Japan Arc, *Geol. Soc. Lond. Spec. Publ.*, *385*, http://dx.doi.org/10.1144/SP385.15.
Yoshii, T. (1975), Proposal of the "aseismic front", *Zisin 2*, *28*, 365–367 (in Japanese).
Yoshii, T. (1979), A detailed cross-section of the deep seismic zone beneath northeastern Honshu, Japan, *Tectonophysics*, *55*, 349–360.
Zhu, G., T. V. Gerya, D. A. Yuen, S. Honda, T. Yoshida, and J. A. D. Connolly (2009), Three-dimensional dynamics of hydrous thermal-chemical plumes in oceanic subduction zones, *Geochem. Geophys. Geosyst.*, *10*, Q11006 doi:10.1029/2009GC002625.

Note Added in Proof

I have realized that my explanation of the formulation of the slab weakening by phase changes is incorrect, and I have found a mis-programming also. However, the difference caused by the mis-programming is small as is shown below, and, therefore, it does not affect the conclusion.

The first sentence of the second paragraph of Appendix A should read:

"The law of viscosity is the type (A), $\eta_{\rm A}$, as described in Honda (2016a)"

The part from Eq. (A.1) to the end of the second paragraph should read:

"

$$\eta = \eta\,(T,z)_{\rm A} \times \begin{cases} r_{\rm PH}^{p_m} \;\; (T \le T_{\rm min}) \\ r_{\rm PH}^{\left(\frac{T-T_{\rm max}}{T_{\rm min}-T_{\rm max}}\right)p_m} \;\; (T_{\rm min} < T < T_{\rm max})\,, \\ 1 \;\; (T \ge T_{\rm max}) \end{cases} \tag{A.1}$$

where η is the viscosity, T is the temperature, z is the depth, $r = 0.01$ and $p_m = 2.5$ are constants, and $T_{\rm max} = 850^\circ$C and $T_{\rm min} = 600^\circ$C. The multiplier of $\eta\,(T,z)_{\rm A}$ is based on the rheological weakening by the grain-size reduction through the phase change (e.g., Čížková *et al.*, 2002; Tagawa *et al.*, 2007; Morishige and Honda, 2013). However, it should be regarded as a parameterization of the rheological weakening of the slab rather than an application of experimental results.

The effective viscosity of the yielded mantle $\eta_{\rm eff}$ is given by

$$\eta_{\rm eff} = \min\left[\eta, \frac{\sigma_B}{2\epsilon}, \frac{\sigma_Y}{2\epsilon}\right] \tag{A.2}$$

where $\epsilon = \sqrt{\epsilon_{ij}\epsilon_{ij}}$ is the second invariant of the strain rate tensor ϵ_{ij} (Tackley, 2000). The depth of the plate boundary (d_p of Honda (2016a)) is set to be 100 km, σ_B is the Byerlee's type frictional stress, and σ_Y ($= \sigma_B$ at $z = d_p$) below a 100 km depth is 500 MPa which is equivalent to the effective friction coefficient of $\sim$0.1 above a 100 km depth. This σ_Y is higher than that used before (100$\sim$200 MPa: Honda, 2014, 2016a) to avoid the break-up of the subducting slab by the hot anomaly (see the arrow in Fig. 18). As a result, rheological weakening of the slab is required for the slab to stagnate in the transition zone, as shown in Fig. A2."

Note that I have slightly changed the magnitude of the hot anomaly from 150 K to 140 K. The correct programming has led to a softer slab. As a result, the slab tends to attach to the upper surface. To avoid this, we have slightly decreased the magnitude of the hot anomaly. This is not the critical point of our conclusion considering the ambiguities of the various parameters.

Page 57 right column line 1: 150 K should be read as 140 K.

Figures relating to these corrections (Figs. 22, A2, A3 and A4) are shown next.

doi:10.5047/meep.2017.00502.0035

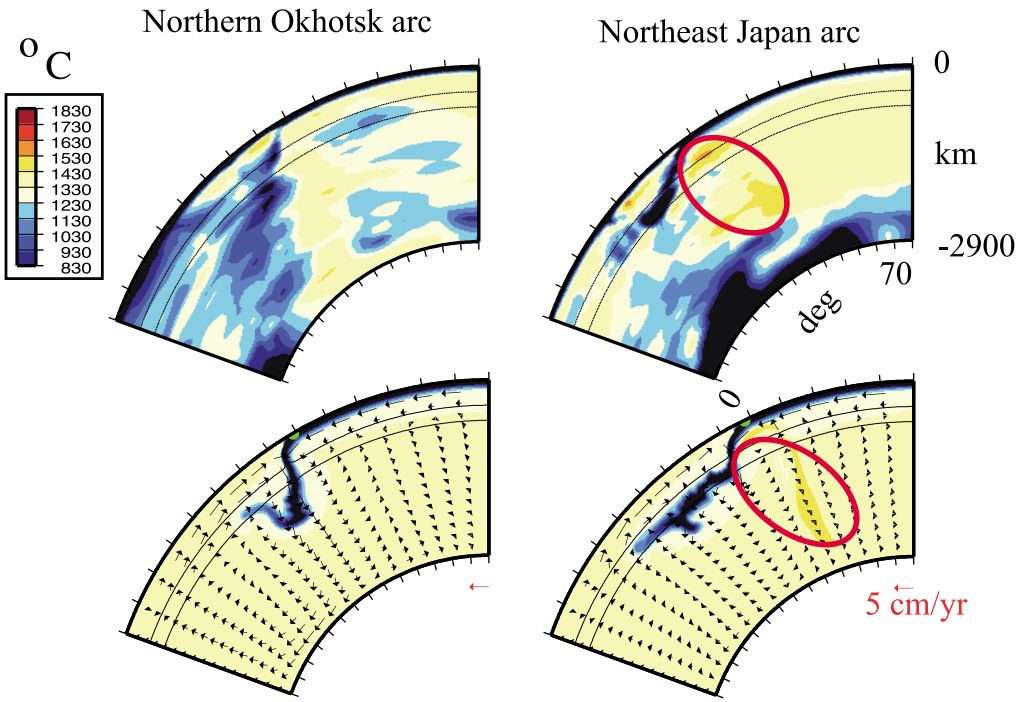

Correct Fig. 22.

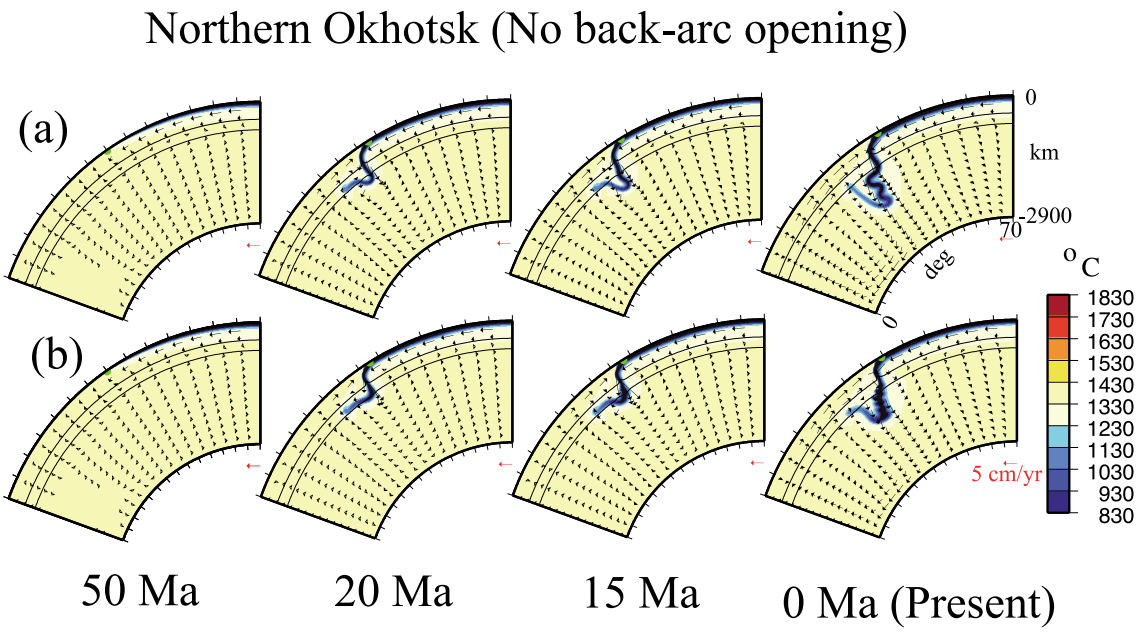

Correct Fig. A2.

doi:10.5047/meep.2017.00502.0035

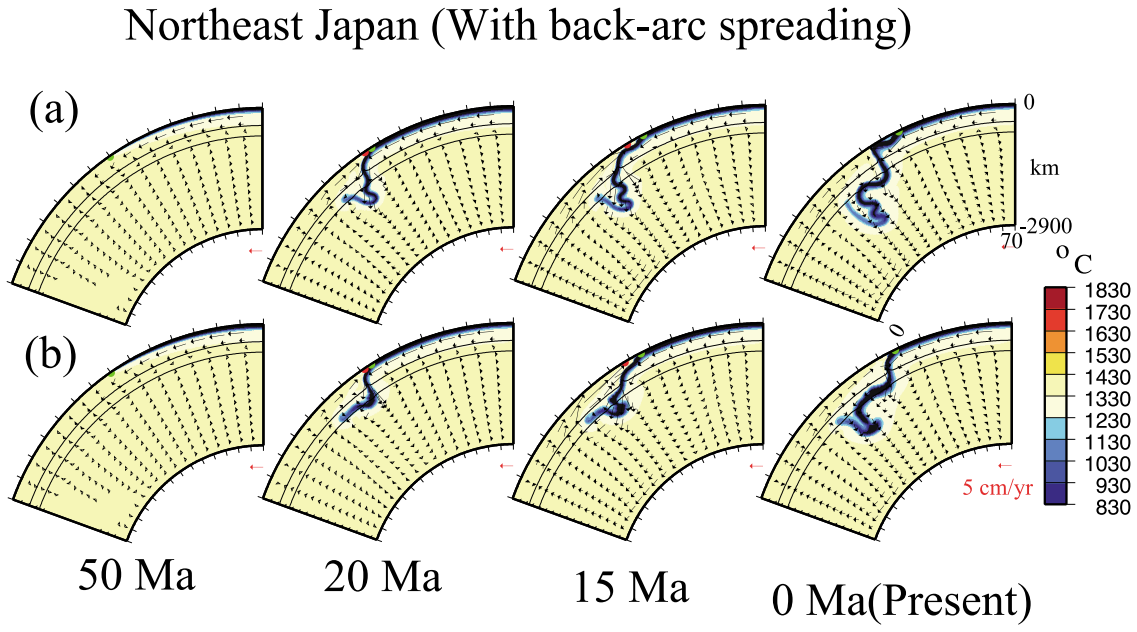

Correct Fig. A3.

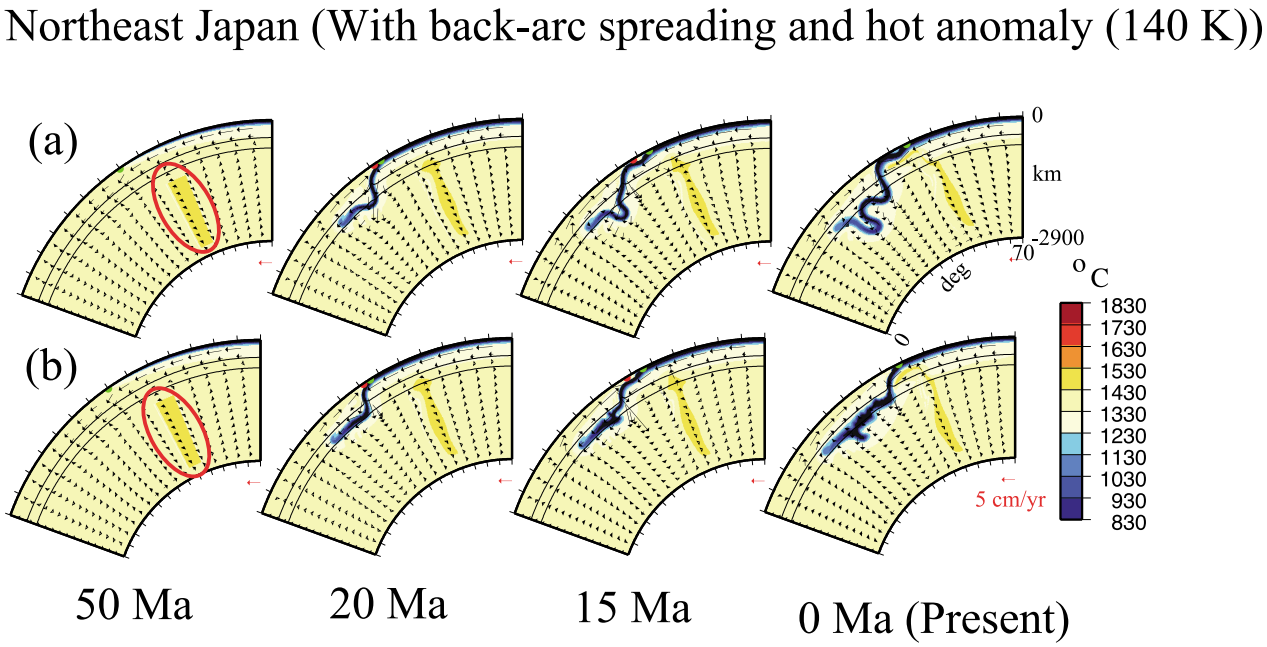

Correct Fig. A4.

doi:10.5047/meep.2017.00502.0035